

# REPORT DOCUMENTATION PAGE

Form Approved  
OMB No. 0704-0188

Public reporting burden for this collection of information is estimated to average 1 hour per response, including the time for reviewing instructions, searching existing data sources, gathering and maintaining the data needed, and completing and reviewing this collection of information. Send comments regarding this burden estimate or any other aspect of this collection of information, including suggestions for reducing this burden to Department of Defense, Washington Headquarters Services, Directorate for Information Operations and Reports (0704-0188), 1215 Jefferson Davis Highway, Suite 1204, Arlington, VA 22202-4302. Respondents should be aware that notwithstanding any other provision of law, no person shall be subject to any penalty for failing to comply with a collection of information if it does not display a currently valid OMB control number. PLEASE DO NOT RETURN YOUR FORM TO THE ABOVE ADDRESS.

1. REPORT DATE (DD-MM-YYYY)		2. REPORT TYPE Technical Papers		3. DATES COVERED (From - To)	
4. TITLE AND SUBTITLE				5a. CONTRACT NUMBER	
				5b. GRANT NUMBER	
				5c. PROGRAM ELEMENT NUMBER	
6. AUTHOR(S)				5d. PROJECT NUMBER 2303	
				5e. TASK NUMBER m2c8	
				5f. WORK UNIT NUMBER	
7. PERFORMING ORGANIZATION NAME(S) AND ADDRESS(ES) Air Force Research Laboratory (AFMC) AFRL/PRS 5 Pollux Drive Edwards AFB CA 93524-7048				8. PERFORMING ORGANIZATION REPORT	
9. SPONSORING / MONITORING AGENCY NAME(S) AND ADDRESS(ES) Air Force Research Laboratory (AFMC) AFRL/PRS 5 Pollux Drive Edwards AFB CA 93524-7048				10. SPONSOR/MONITOR'S ACRONYM(S)	
				11. SPONSOR/MONITOR'S NUMBER(S)	
12. DISTRIBUTION / AVAILABILITY STATEMENT  Approved for public release; distribution unlimited.					
13. SUPPLEMENTARY NOTES					
14. ABSTRACT					
15. SUBJECT TERMS					
16. SECURITY CLASSIFICATION OF:			17. LIMITATION OF ABSTRACT  A	18. NUMBER OF PAGES	19a. NAME OF RESPONSIBLE PERSON Leilani Richardson
a. REPORT Unclassified	b. ABSTRACT Unclassified	c. THIS PAGE Unclassified			19b. TELEPHONE NUMBER (include area code) (661) 275-5015

62

1121 031  
separate items are enclosed

2203M2C8  
NOTIFIED/FILE

MEMORANDUM FOR PR (In-House Publication)

03 November 1999

FROM: PROI (TI) (STINFO)

SUBJECT: Authorization for Release of Technical Information, Control Number: **AFRL-PR-ED-TP-1999-0209**  
Sogoshi, N., Tam, S., et al., "High Resolution Infrared Absorption Spectroscopy of C60 Molecules and  
Clusters in Parahydrogen Solids"  
**Journal of Physical Chemistry**

---

(Statement A)

# High Resolution Infrared Absorption Spectroscopy of C<sub>60</sub> Molecules and Clusters in Parahydrogen Solids

Norihito Sogoshi, Yoshiyasu Kato, Tomonari Wakabayashi and Takamasa Momose<sup>a)</sup>  
Department of Chemistry, Graduate School of Science, Kyoto University,  
and Japan Science and Technology Corporation (JST), Kyoto 606-8502, Japan

and

Simon Tam, Michelle E. DeRose, and Mario E. Fajardo<sup>b)</sup>  
Propulsion Directorate, US Air Force Research Laboratory  
AFRL/PRSP, Bldg. 8451, Edwards AFB, CA 93524-7680

a) email: momose@kuchem.kyoto-u.ac.jp

b) email: mario\_fajardo@ple.af.mil

Submitted to J. Phys. Chem. \_\_\_\_\_, Received \_\_\_\_\_, Accepted \_\_\_\_\_

## ABSTRACT

We report the isolation of C<sub>60</sub> molecules in cryogenic pH<sub>2</sub> solids by the rapid vapor deposition method. New theoretical simulations of rovibrational spectra for low temperature isolated <sup>12</sup>C<sub>60</sub> molecules, including boson-exchange symmetry restrictions on the rotational levels, predict a characteristic "null gap" and unequal rotational line spacings for low-*J* values. High resolution (IR) absorption spectra of the C<sub>60</sub>/pH<sub>2</sub> samples failed to show rotationally resolved features, and in fact suggest that the majority of the C<sub>60</sub> molecules are not rotating. However, spectra of the *F*<sub>1u</sub>(1) vibrational mode near 530 cm<sup>-1</sup> show linewidths of ≈ 0.2 cm<sup>-1</sup> (FWHM), the sharpest IR absorption bands for C<sub>60</sub> reported to date. Visible absorption spectra also show sharp features in the ≈ 600 nm region, supporting our contention of well isolated C<sub>60</sub> molecules. The C<sub>60</sub> molecules appear to stabilize the pH<sub>2</sub> solid, inhibiting the fcc to hcp conversion which usually occurs upon annealing of rapid vapor deposited pH<sub>2</sub> solids to T ≈ 5 K. We also report surprisingly strong C<sub>60</sub>-induced IR activity in the pH<sub>2</sub> solid, and propose this phenomenon as a diagnostic for H<sub>2</sub> molecules adsorbed by carbon nanotubes. C<sub>60</sub>/pH<sub>2</sub> samples grown in an enclosed cell by laser ablation of solid C<sub>60</sub> appear to contain predominantly (C<sub>60</sub>)<sub>n</sub> clusters; these clusters are too small to exhibit "bulk" vibrational or electronic properties, as determined by IR and UV/visible absorption spectroscopies. Future experiments to disentangle the contributions of <sup>13</sup>C isotopic substitution, pH<sub>2</sub> matrix effects, and the putative hindered rotation of C<sub>60</sub> molecules to the observed C<sub>60</sub>/pH<sub>2</sub> IR lineshapes are presently under consideration.

20021121 031

## I. INTRODUCTION

The fullerene literature has grown to over fifteen thousand publications,<sup>1</sup> encompassing early theoretical speculations<sup>2</sup> and predictions,<sup>3</sup> the mass spectrometric detection of buckminsterfullerene ( $C_{60}$ ) and other fullerene molecules,<sup>4,5</sup> the production of macroscopic quantities of purified fullerenes,<sup>6</sup> the discovery of carbon nanotubes,<sup>7,8</sup> and a rapidly expanding number of more recent developments.<sup>9-11</sup> This profusion of activity reflects the diverse and multidisciplinary nature of fullerene research. In particular, the highly symmetrical truncated icosahedron  $C_{60}$  molecule has captured the imaginations of researchers in fields including: molecular spectroscopy, solid state physics, interstellar chemistry, and materials science.

In this manuscript, we describe the application of high resolution infrared (IR) absorption spectroscopy to the study of  $C_{60}$  molecules and clusters trapped in cryogenic parahydrogen ( $pH_2$ ) solids. Improved spectroscopic data for the isolated  $C_{60}$  molecule could yield more precise knowledge of its equilibrium structure and rovibrational dynamics<sup>13-18</sup>, providing new benchmarks against which further improvements in theory could be measured; our ultimate goal is the observation and assignment of a rotationally resolved spectrum. Spectroscopic data on  $C_{60}$  van der Waals dimers and larger clusters in principle contain information about  $C_{60}$ - $C_{60}$  interactions, which could illuminate lattice vibrational and rotational dynamics in pure and doped  $C_{60}$  solids. Spectral features attributable to the presence of the  $pH_2$  matrix host contain information about the structure(s) of the  $C_{60}/pH_2$  trapping site(s) and the van der Waals interaction potential between  $C_{60}$  and  $H_2$  molecules. An improved  $C_{60}$ - $H_2$  interaction potential could assist efforts to model the adsorption of  $H_2$  by carbon nanotubes,<sup>19-21</sup> currently under investigation as a practical method for hydrogen fuel storage.

The theoretical groundwork for assigning a rotationally resolved electronic or vibrational spectrum of a low temperature  $C_{60}$  sample has been well prepared.<sup>13,14,22-26</sup> However, despite the vastness of the fullerene literature, none of the reported experimental spectra show linewidths or peak spacings characteristic of rotationally resolved features (*vide infra*). Gas phase IR emission measurements on samples at  $T \approx 1000$  K reveal only  $\sim 10$   $cm^{-1}$  full-width-at-half-maximum (FWHM) unresolved bands.<sup>27</sup> The cold molecular beam electronic (resonant two-photon ionization, R2PI) spectrum of  $C_{60}$  at  $T \sim 100$  K shows sharp vibronic features with linewidths comparable to the 3  $cm^{-1}$  experimental resolution.<sup>28</sup> The electronic absorption spectrum of  $C_{60}$  isolated in helium droplets<sup>29</sup> at  $T \approx 0.4$  K shows lines as sharp as 1.5  $cm^{-1}$  FWHM, and is very

similar to the molecular beam R2PI spectrum. Several reports of electronic absorption and emission spectra of  $C_{60}$  isolated in cryogenic rare gas matrices have appeared,<sup>30-34</sup> with no sign of rotational structure or peaks narrower than  $\sim 10 \text{ cm}^{-1}$  FWHM. These vibronic features appear even less well resolved in electronic spectra of  $C_{60}$ /hydrocarbon solutions<sup>35-39</sup> and cryogenic glasses.<sup>40</sup> IR absorption studies of matrix isolated  $C_{60}$  are badly underreported;<sup>41</sup> the narrowest line in this early  $C_{60}$ /Ar study is the  $1 \text{ cm}^{-1}$  FWHM  $F_{1u}(1)$  absorption at  $530.1 \text{ cm}^{-1}$ . IR absorption<sup>6,41-52</sup> and Raman scattering<sup>42,43,47,53-59</sup> spectroscopies are widely employed as probes of  $C_{60}$  solids. The narrowest reported IR absorption feature is the  $0.5 \text{ cm}^{-1}$  FWHM  $F_{1u}(2)$  absorption at  $576.5 \text{ cm}^{-1}$  in a 15 K solid  $C_{60}$  sample.<sup>43</sup> Raman spectra of  $C_{60}$  solids cooled to  $T \approx 2 \text{ K}$  show much sharper fine structure,<sup>55,58</sup> with individual components having linewidths as narrow as  $0.1 \text{ cm}^{-1}$ ; the various features are sensitive to the samples' isotopic compositions and/or degree of orientational disorder. Vibrational transitions of  $C_{60}$  in liquid solutions<sup>43,60-62</sup> and in solid phase compounds<sup>63-66</sup> typically show linewidths of  $\approx 1 \text{ cm}^{-1}$  FWHM, or larger.

*one or  
word  
hyphenated*

The phenomenon of high resolution IR spectroscopy in doped  $pH_2$  solids was discovered by Oka and co-workers at the University of Chicago,<sup>67</sup> and further developed in collaboration with Shida, Momose and co-workers at Kyoto University.<sup>68-74</sup> Two suggestive examples: linewidths as narrow as  $0.0003 \text{ cm}^{-1}$  are observed for the  $Q_1(0)$  transition of isolated  $D_2$  molecules;<sup>67</sup> the  $\nu_4$  band of  $CH_4/pH_2$  shows that the  $CH_4$  molecules exist as very slightly hindered rotors, with rovibronic spectral features as narrow as  $0.003 \text{ cm}^{-1}$ .<sup>71</sup> The spherical nature of the ground state ( $v=0, J=0$ )  $pH_2$  molecule, the weak attractive  $pH_2$ - $pH_2$  interactions, and the small  $H_2$  mass all contribute to make solid  $pH_2$  a very "soft" matrix host, reducing the incidence and importance of inhomogeneities in a guest molecule's environment. Recently, Fajardo and Tam at Edwards Air Force Base demonstrated the efficient isolation of various atomic and molecular dopants by rapid vapor deposition of the  $pH_2$  solid.<sup>75,76</sup> In a recent collaborative study,<sup>77</sup> we demonstrated the combination of high resolution IR spectroscopy and rapid vapor deposition of  $CH_4$  doped  $pH_2$  solids, obtaining very similar results to the previous  $CH_4/pH_2$  study. This favorable outcome motivated the present investigation of the possibility of observing rotationally resolved spectra of  $C_{60}$  molecules isolated in solid  $pH_2$ .

In what follows we report our preliminary results on the spectroscopy of  $C_{60}/pH_2$  solids. We begin with theoretical predictions of possible rovibrational absorption spectra of isolated  $C_{60}$  molecules at liquid helium temperatures. We give a qualitative argument for the possibility of

isolating  $C_{60}$  molecules in fairly small, high symmetry trapping sites in the  $pH_2$  solid; sites in which the  $C_{60}$  molecules might exist as slightly hindered rotors. We describe our experimental apparatus and procedures and present the results of various spectroscopic measurements on  $C_{60}/pH_2$  solids. While we do not observe rotationally resolved spectra, we do report the narrowest IR absorption features for  $C_{60}$ , to date. We discuss these results in the context of the issues raised above. Experiments to determine the influences of the  $^{13}C$  isotopic composition of our  $C_{60}$  samples, of spectral perturbations induced by the  $pH_2$  host, and of possible rotation of the trapped  $C_{60}$  molecules, are still in progress. Accordingly those results, and a detailed final analysis of our IR absorption lineshapes, will be postponed until a later publication.

## II. THEORY

### A. Rovibrational States of $^{12}C_{60}$

The buckminsterfullerene ( $C_{60}$ ) molecule has a hollow-cage, nearly spherical shape with icosahedral ( $I_h$ ) symmetry.<sup>9-11</sup> Because of this highly symmetrical structure, many of its physical and chemical properties are quite unique. For instance, among the 174 vibrational degrees of freedom, there are only 46 distinct vibrational frequencies, and only the ~~4~~<sup>four</sup> modes of  $F_{1u}$  symmetry are IR active.<sup>23</sup>

$C_{60}$  is a spherical top rotor with a small rotational constant of  $B \approx 0.0028 \text{ cm}^{-1}$ ; thus, even at temperatures below 10 K a large number of rotational levels will be occupied. However, in the specific case of the  $^{12}C_{60}$  molecule (*i.e.*: all ~~sixty~~<sup>60</sup> carbon atoms are the  $^{12}C$  isotope), boson-exchange symmetry restrictions require that many of the rotational quantum levels do not exist.<sup>23</sup> These predicted "missing" levels result in a characteristic pattern of spectral line spacings which we expect will be key to observing and assigning a rotationally resolved  $C_{60}$  spectrum. We will address the effects of  $^{13}C$  isotopic substitutions in a subsequent section.

In  $^{12}C_{60}$ , all 60 carbon nuclei have zero spin. The total wavefunction  $\Psi_{el}\Psi_{vib}\Psi_{rot}\Psi_{ns}$  must be invariant under any permutation of  $^{12}C$  nuclei, where  $\Psi_{el}$ ,  $\Psi_{vib}$ ,  $\Psi_{rot}$ , and  $\Psi_{ns}$  denote the electronic, vibrational, rotational, and nuclear-spin wavefunctions, respectively. Since the molecule has one possible nuclear-spin wavefunction of  $A_g$  symmetry in the point group  $I_h$ , and since the IR absorption occurs in the ground electronic state of  $A_g$  symmetry, the rovibrational wavefunction  $\Psi_{vib}\Psi_{rot}$  should have  $A_g$  or  $A_u$  symmetry.<sup>78,79</sup>

To find the allowed rotational levels satisfying these boson-exchange symmetry restrictions, it is convenient to consider irreducible representations in the pure rotational subgroup of  $I_h$ ; that is in  $I$ , where  $I_h = I \otimes i$ , with  $i$  being the inversion operation. Then the rovibrational wavefunction  $\Psi_{\text{vib}}\Psi_{\text{rot}}$  should have  $A$  symmetry in  $I$ . In the case of the vibrational ground state where  $\Psi_{\text{vib}}$  has  $A_g$  symmetry in  $I_h$ , the possible rotational states  $\Psi_{\text{rot}}$  are those of  $A$  symmetry in  $I$ . Thus, the allowed rotational levels are: only 1 level among each of  $J = 0, 6, 10, 12, 15, 16, 18, 20, 21, 22, 24-28$ , and  $31-35$ ; and 2 levels among each of  $J = 30$  and  $36$  and so on.<sup>23</sup> The rotational levels of  $J = 1-5, 7-9, 11, 13, 14, 17, 19, 23$ , and  $29$  are all missing in the ground vibrational state. For example, in the case of  $J = 5$  there are  $2(5)+1 = 11$  conceivable rotational levels having  $F_1 \oplus F_2 \oplus H$  symmetry in  $I$ , but none of them is allowed in the vibrational ground state of  $^{12}\text{C}_{60}$ . On the other hand, in the case of the vibrationally excited states of  $F_{1u}$  symmetry, it is found that the allowed rotational levels are: 1 level among each of  $J = 1, 5-7, 9, 10, 12-14$ , and  $18$ ; and 2 levels among each of  $J = 11, 15-17$ , and  $19$ , and so on. The rotational levels of  $J = 0, 2-4$ , and  $8$  are all missing in the  $F_{1u}$  vibrational excited state. For example,  $3(2(5)+1) = 33$  levels are conceivable for  $J = 5$  rovibrational levels; they have  $F_1 \otimes (F_1 \oplus F_2 \oplus H) = A \oplus 2F_1 \oplus F_2 \oplus 2G \oplus 3H$  symmetry in  $I$ . Among them, only one rovibrational level with  $A$  symmetry is allowed for  $^{12}\text{C}_{60}$ .

The rovibrational Hamiltonian of  $^{12}\text{C}_{60}$  is that of a spherical top molecule.<sup>78</sup> The ground state energies can be expressed as  $BJ(J+1)$ , where  $J$  is the rotational quantum number. In the case of the triply degenerate  $F_{1u}$  vibrational excited states, the degeneracy is lifted into three levels due to the Coriolis coupling interaction. By denoting the vibrational, rotational, and total angular momenta as  $l$ ,  $R$ , and  $J = l + R$ , respectively, the rovibrational energies of each level can be expressed as follows:<sup>78</sup>

$$F_{1u}^{(-)}(J) = \nu_{\text{vib}} + BJ(J+1) - 2B\zeta J \quad \text{for } R=J-1 \quad (1a)$$

$$F_{1u}^{(0)}(J) = \nu_{\text{vib}} + BJ(J+1) \quad \text{for } R=J \quad (1b)$$

$$F_{1u}^{(+)}(J) = \nu_{\text{vib}} + BJ(J+1) + 2B\zeta(J+1) \quad \text{for } R=J+1 \quad (1c)$$

where  $\nu_{\text{vib}}$  and  $\zeta$  are the band origin and the Coriolis coupling constant, respectively. Note that the vibrational angular momentum of the  $F_{1u}$  state is  $l = 1$ . The magnitude and the sign of the



Coriolis coupling constant  $\zeta$  depends on the vibrational mode and should be determined experimentally, which is yet to be done. Calculated values<sup>13</sup> for the four  $F_{lu}$  modes of  $C_{60}$  are:  $\zeta_1 = -0.107$  for  $F_{lu}(1)$  at  $530 \text{ cm}^{-1}$ ,  $\zeta_2 = -0.498$  for  $F_{lu}(2)$  at  $578 \text{ cm}^{-1}$ ,  $\zeta_3 = -0.319$  for  $F_{lu}(3)$  at  $1184 \text{ cm}^{-1}$ , and  $\zeta_4 = -0.076$  for  $F_{lu}(4)$  at  $1432 \text{ cm}^{-1}$ . Note that these values satisfy the relation:  $\sum \zeta_i(F_{lu}) = -1$ . In Figure 1, the rotational energy levels for the upper  $F_{lu}$  and lower  $A_g$  vibrational states of  $^{12}C_{60}$  are depicted with the assumption of  $\zeta < 0$ . The IR allowed transitions are also shown by arrows where the selection rule is  $\Delta R = 0$ . It is seen that the P branch is composed of the transitions to  $F_{lu}^{(+)}$  levels, the Q branch to  $F_{lu}^{(0)}$  levels, and the R branch to  $F_{lu}^{(-)}$  levels, respectively.

The rotational population distribution  $P(J)$  for a spherical top molecule at a given temperature  $T$  is proportional to the Maxwell-Boltzmann factor:<sup>78</sup>

$$P(J) \propto (2J+1) g(J) \exp[-BJ(J+1)hc/kT] \quad (2).$$

The first term of the right-hand side,  $2J+1$ , corresponds to the degeneracy of  $J$  projected along a space fixed axis. The second factor  $g(J)$  corresponds to the degeneracy of  $J$  projected along a molecule fixed axis. Without the boson-exchange symmetry restrictions,  $g(J)$  is equal to  $2J+1$ . However, as mentioned above, the boson-exchange symmetry restrictions requires that for the ground state of  $^{12}C_{60}$  the factor should be  $g(J) = 0$  for  $J = 1-5, 7-9, 11, \dots$ ;  $g(J) = 1$  for  $J = 0, 6, 10, \dots$ ;  $g(J) = 2$  for  $J = 30, 36, 40, \dots$ , and so on. The relative intensities of the rovibrational absorption lines are calculated from the ground state population  $P(J)$ .

Figure 2 shows calculated spectral lineshapes for an IR active transition  $F_{lu} \leftarrow A_g$  of  $^{12}C_{60}$  at  $T = 5.0 \text{ K}$  and  $2.5 \text{ K}$ . The rotational constant of  $B = 0.0028 \text{ cm}^{-1}$  is assumed for both the upper  $F_{lu}$  and lower  $A_g$  vibrational states. The Coriolis coupling constant for the upper state is taken as  $\zeta_3 = -0.319$ , which is the calculated value<sup>13</sup> for the  $F_{lu}(3)$  mode at  $1184 \text{ cm}^{-1}$ . The most obvious feature of this simulated spectrum is the very strong, sharp, overlapped Q-branch feature (see insets) which results from the assumption of equal rotational constants for upper and lower vibrational states. More revealing is the unevenly spaced pattern of rotational lines in the low- $J$  portions of the P and R-branches which reflects the missing rotational levels. At high- $J$  regions a spacing of  $\Delta = 2 B (1-\zeta) = 0.0074 \text{ cm}^{-1}$  is seen between adjacent spectral lines.



Figure 3 shows the results of a nearly identical pair of calculations, except that the rotational constant of the excited vibrational state is assumed to be 1% smaller than in the ground state. The corresponding increase in the molecule's moment of inertia requires a radial enlargement upon vibrational excitation of the C<sub>60</sub> cage by 0.5% ( $\approx 0.02$  Å), and a 0.5% increase in all the C-C bond lengths ( $\approx 0.007$  Å); similar anharmonic distortions have been considered before.<sup>25</sup> In this case the Q-branch transitions are not all coincident, and the missing level "null-gap" between the P and Q-branches is obliterated. However, for the R-branch the characteristic null-gap and unevenly spaced rotational line pattern survives intact.

*close up  
number &  
plus sign*

Anticipating the possibility that individual rotational lines may not be resolved in a given experiment, Figure 4 shows the results of the same spectral simulations as in Figure 3, except at a degraded spectral resolution of 0.05 cm<sup>-1</sup> FWHM. The bandshapes are qualitatively similar to those calculated for C<sub>70</sub> using comparable assumptions.<sup>26</sup> Note that the difference spectrum, trace (b)-(a), is plotted on the same vertical scale as the simulated spectra. Thus, absent the direct observation of rotationally resolved features, we expect strong temperature induced changes to the rotational envelope over a  $\approx 1.5$  cm<sup>-1</sup> region as a signature of rotating C<sub>60</sub> molecules. We compare the results of this simulation directly to our experimental data below.

## B. <sup>13</sup>C Isotopic Substitution

In contrast to icosahedral <sup>12</sup>C<sub>60</sub>, the <sup>13</sup>C<sup>12</sup>C<sub>59</sub> molecule has only C<sub>s</sub> symmetry,<sup>23</sup> and its rotational levels are those of a slightly prolate symmetric top, without the strict bosonic-exchange exclusion.<sup>23,24</sup> The extra neutron also lifts the three-fold degeneracy of the four F<sub>1u</sub> vibrational modes<sup>14</sup> by amounts ranging from  $\approx 0.5$  to over 2 cm<sup>-1</sup>. For <sup>13</sup>C<sub>2</sub><sup>12</sup>C<sub>58</sub>, there are three possible symmetries: C<sub>1</sub>, C<sub>s</sub>, and C<sub>2v</sub> occurring with probabilities: 56/59, 1/59, and 2/59, respectively.<sup>23</sup> Thus, for the vast majority of <sup>13</sup>C<sub>2</sub><sup>12</sup>C<sub>58</sub> molecules, there are no symmetry restrictions on the rotational and vibrational states.<sup>23</sup>

The probabilities of a C<sub>60</sub> molecule containing exactly n <sup>13</sup>C atoms is given by the Bernoulli Trials formula:<sup>24</sup>

$$P(p,n) = \frac{60!}{n!(60-n)!} p^n (1-p)^{60-n} \quad (3).$$

For the natural  $^{13}\text{C}$  isotopic abundance of  $p = 0.011$ , the relative concentrations of  $^{12}\text{C}_{60}$ ,  $^{13}\text{C}^{12}\text{C}_{59}$ , and  $^{13}\text{C}_2^{12}\text{C}_{58}$  are:  $\approx 0.51$ ,  $0.34$ , and  $0.11$ , respectively. Thus, the experimental spectrum of a natural isotopic abundance  $\text{C}_{60}$  sample will be a superposition of the  $^{12}\text{C}_{60}$ ,  $^{13}\text{C}^{12}\text{C}_{59}$ , and  $^{13}\text{C}_2^{12}\text{C}_{58}$  spectra, weighted by their relative concentrations. This will seriously complicate the analysis of any vibrational spectrum, since nearly half of the  $\text{C}_{60}$  molecules will include at least one  $^{13}\text{C}$  atom.

### C. $\text{C}_{60}$ Trapping Sites in Solid $\text{pH}_2$

Unlike the previously well-studied<sup>70-72,77</sup> example of  $\text{CH}_4/\text{pH}_2$ , the  $\text{C}_{60}$  molecule is far too large to fit into a single substitutional site in the  $\text{pH}_2$  solid. We can estimate the size of the vacancy in solid  $\text{pH}_2$  required to accommodate a  $\text{C}_{60}$  molecule as the ratio of the molecular volumes calculated according to:

$$N_{\text{vac}} \approx \left( \frac{R_e(\text{C}_{60} - \text{pH}_2)}{R_{\text{nn}}(\text{pH}_2)} \right)^3 \quad (4)$$

in which:  $R_e(\text{C}_{60} - \text{pH}_2)$  is the separation at the  $\text{C}_{60} - \text{pH}_2$  potential minimum, and  $R_{\text{nn}}(\text{pH}_2) \approx 3.79$  Å is the nearest neighbor separation in solid  $\text{pH}_2$  at liquid helium temperatures.<sup>80</sup> The use of  $R_{\text{nn}}(\text{pH}_2)$  instead of  $R_e(\text{pH}_2 - \text{pH}_2)$  in Eqn. (4) is intended to include quantum zero-point motion effects on the structure of solid  $\text{pH}_2$ , effects neglected in a simple potential energy minimization. This formula<sup>81</sup> for  $N_{\text{vac}}$  has yielded reasonable agreement with the results of Monte Carlo simulations of relaxed Li atom trapping sites in rare gas<sup>82</sup> and  $\text{pH}_2$  solids.<sup>83,84</sup>

Unfortunately, we could not find a  $\text{C}_{60} - \text{pH}_2$  van der Waals interaction potential in the literature, so we estimate  $R_e(\text{C}_{60} - \text{pH}_2)$  by averaging<sup>85</sup> the minimum separations of the  $\text{pH}_2 - \text{pH}_2$  and  $\text{C}_{60} - \text{C}_{60}$  interaction potentials:<sup>80,86</sup>  $R_e(\text{C}_{60} - \text{pH}_2) \approx \frac{1}{2} \{R_e(\text{C}_{60} - \text{C}_{60}) + R_e(\text{pH}_2 - \text{pH}_2)\} \approx \frac{1}{2} \{10.06 \text{ Å} + 3.41 \text{ Å}\} \approx 6.7 \text{ Å}$ . This value is in reasonable agreement with the sum of the radius of the  $\text{C}_{60}$  cage<sup>86</sup> and a typical adsorption separation for  $\text{H}_2$  on graphite:<sup>19</sup>  $3.55 \text{ Å} + 2.95 \text{ Å} = 6.5 \text{ Å}$ . Thus, Eqn. (4) predicts that a vacancy formed by removing approximately 6  $\text{pH}_2$  molecules is required to accommodate each  $\text{C}_{60}$  molecule.

Candidates for highly symmetrical 6-vacancies in close packed  $\text{pH}_2$  solids can be generated by removing the  $\text{pH}_2$  molecules immediately surrounding the "octahedral" interstitial sites.<sup>87</sup> In

face centered cubic (fcc) solid  $pH_2$ , such a 6-vacancy site would have true  $O_h$  symmetry. However in hexagonal close packed (hcp) solid  $pH_2$ , which is anisotropic, the site symmetry is reduced to  $D_{3d}$ . Numerous other plausible trapping site structures of lower symmetry can be proposed. We simply note that the possibility of trapping  $C_{60}$  molecules in well defined, highly symmetrical sites encourages our expectations of sharp spectral features, and possibly even the existence of  $C_{60}$  molecules as slightly hindered rotors.

### III. EXPERIMENTAL

Both experimental apparatus have been described in detail before,<sup>68,69,71,73-77</sup> here we give a brief summary, highlighting important modifications and additions.

#### A. Rapid Vapor Deposition

Doped  $pH_2$  solids are prepared by rapid vapor deposition of precooled  $pH_2$  gas and hot  $C_{60}$  vapor onto a CsI substrate cooled to  $T \approx 2$  K in a  $^4He$  bath cryostat. We operate the ortho/para (o/p) converter at 15 K, with  $nH_2$  inlet rates between 25 and 50 mmol/h, yielding a flow of precooled 99.99 %  $pH_2$  which impinges upon the substrate at a  $45^\circ$  angle. During deposition the pressure of uncondensed  $pH_2$  gas remains below  $\sim 10^{-4}$  Torr. The  $C_{60}$  dopant (Aesar 99.5 %) is vaporized in a stainless steel Knudsen oven<sup>88</sup> operated at temperatures between 820 and 850 K, resulting in  $C_{60}$  vapor pressures<sup>89-92</sup> of  $\sim 10^{-2}$  Torr. Higher oven temperatures are avoided in order to minimize chemical reaction of the  $C_{60}$  with the uncondensed  $H_2$  gas.<sup>93</sup> The 1.5 mm diameter oven orifice is situated 5 cm from the center of the CsI substrate at an angle of  $45^\circ$  from the substrate surface normal, at  $90^\circ$  to the  $pH_2$  source.

We record IR absorption spectra of our  $C_{60}/pH_2$  samples at resolutions of 0.1 and 0.01  $cm^{-1}$  along the substrate normal. The FTIR spectrometer (Bruker IFS120HR) is equipped with a glowbar source, a KBr beamsplitter, and three detectors: InSb (1800 to 9000  $cm^{-1}$ ), HgCdTe (550 to 7900  $cm^{-1}$ ), and a Si bolometer (400 to 700  $cm^{-1}$ ). Visible absorption spectra are recorded using a tungsten filament lamp source, and an optical multichannel analyzer equipped with an intensified silicon diode array detector mounted on a 275 mm focal length triple grating polychromator. The instrumental linewidth is  $\approx 0.8$  nm FWHM as measured using the Hg lamp calibration lines. To accommodate the IR diagnostic, the  $^4He$  cryostat resides inside a 0.5  $m^3$  polycarbonate box purged with a constant flow of dry  $N_2$  gas.

## B. Enclosed Cell Condensation

$C_{60}$  doped  $pH_2$  solids are prepared by co-condensation in an enclosed cell, as reported previously.<sup>73,77</sup> Normal hydrogen ( $nH_2$ ) gas is converted to pure  $pH_2$  in advance and kept in a tank at room temperature. The  $pH_2$  gas is introduced through a thin stainless steel inlet tube into a copper cell cooled by a liquid helium (lHe) bath cryostat; the inlet gas flow rate is typically  $\approx$  300 mmol/h.  $C_{60}$  is volatilized inside the copper cell by pulsed laser ablation.<sup>69</sup> A 15 mm diameter by 2 mm thick solid  $C_{60}$  target disk is formed by pressing  $C_{60}$  powder onto an aluminum plate at  $P \sim 20$  kgw/cm<sup>2</sup>. During the  $pH_2$  condensation, a pulsed laser beam from a Nd:YLF laser (Spectra Physics TFR:  $\lambda = 523.5$  nm,  $\approx 0.2$  mJ/pulse, 1 kHz repetition rate) is focused on the surface of the  $C_{60}$  target using a 10 cm focal length lens.

don't  
break  
symbol  
and  
quantity

The copper sample cell has an inner diameter of 2 cm and an optical pathlength of 3.0 cm with  $BaF_2$  windows at both ends sealed with indium gaskets. The temperature of the sample cell is kept around 8.5 K during the 1.5 hour long sample preparation. The sample is then cooled to 4.5 K for observation. The doped  $pH_2$  solid grows radially inward from the cell walls and forms a polycrystalline aggregate of hcp crystals having their c-axes normal to the wall of the cell.<sup>67,73</sup> The sample thus grown is completely transparent.

IR absorption spectra are obtained with a Fourier transform infrared (FTIR) spectrometer (Bruker IFS120HR). A glowbar source, a KBr beamsplitter, and a liquid nitrogen ( $lN_2$ ) cooled HgCdTe detector, are employed to acquire spectra at resolutions of 0.25 and 0.01 cm<sup>-1</sup>. UV/visible absorption spectra were recorded using a vacuum UV spectrometer (Jasco VUV-1C, 180-350 nm) and a visible spectrometer (Spex model 1680, 350-820 nm) with a spectral resolution of  $\approx 0.2$  nm.

## IV. RESULTS & DISCUSSION

### A. Isolated $C_{60}$ Molecules

Figures 5 through 8 show absorption spectra of the four dipole allowed  $F_{1u}$  vibrational modes of  $C_{60}$  molecules isolated in rapid vapor deposited  $pH_2$  solids. The  $C_{60}$  concentrations are estimated as  $\approx 100$  PPM, assuming a value for the integrated absorption coefficient of the  $F_{1u}(3)$  mode of  $\int \alpha(\bar{\nu}) d\bar{\nu} = 25$  km/mol.<sup>15,94</sup> The samples also contain  $\sim 1$  PPM of  $H_2O$  and  $CO_2$  as contaminants. In each figure, trace (a) is for the as-deposited sample at  $T = 2.4$  K, trace (b) is for

the sample warmed to  $T = 4.8$  K, and trace (c) is for the "annealed" sample cooled back to  $T = 2.4$  K. To the best of our knowledge, the  $\approx 0.2$  cm<sup>-1</sup> FWHM peaks in the spectra of the  $F_{1u}(1)$  mode constitute the sharpest IR absorption features ever reported for the  $C_{60}$  molecule.

The difference traces in Figures 5 through 8 labeled "(c) - (a)" show the effects of the complete "annealing" temperature cycle, corresponding to irreversible changes in the environments of the  $C_{60}$  molecules, *e.g.*:  $C_{60}$  clustering and/or changes to the  $pH_2$  host. Our previous experiments on pure,<sup>75</sup> and 10 to 100 PPM  $CH_4$  doped,<sup>77</sup> rapid vapor deposited  $pH_2$  solids have demonstrated that the as-deposited samples have a mixed fcc/hcp structure which anneals nearly completely to hcp upon warming to  $T \approx 5$  K. This conversion is accompanied by pronounced changes to the rovibrational spectrum of the trapped  $CH_4$  molecules.<sup>77</sup> In the present case of  $\sim 100$  PPM  $C_{60}/pH_2$  samples, the annealing process appears ineffectual, with very little resulting changes to the absorption lineshapes.

Not shown are spectra of the  $CH_4$   $\nu_4$  band region for another  $C_{60}/pH_2$  sample produced using a higher Knudsen oven temperature; the  $CH_4$  ( $\sim 1$  PPM) is presumably produced in the Knudsen oven by reactions with uncondensed  $pH_2$  gas. Annealing of that sample failed to induce the expected fcc to hcp transformation, as revealed by the  $CH_4$  spectroscopy. The fcc to hcp conversion most likely proceeds by the relative slipping motion of adjacent close packed planes. Apparently the  $CH_4$  molecules, which fit into single substitutional sites, do not hinder this process; whereas the larger  $C_{60}$  molecules, which intrude into adjacent close-packed planes, inhibit their relative motion. The presence of residual inhomogeneous line broadening due to the mixed fcc/hcp structure implies that even sharper spectral features may be obtainable in  $C_{60}/pH_2$  solids prepared under different conditions.

The difference traces in Figures 5 through 8 labeled "(c) - (b)" show the effects of cooling the samples back down from 4.8 to 2.4 K. We expect these difference traces to include signs of both irreversible and reversible changes to the samples, *i.e.*: the final phases of the annealing process, and any possible temperature induced changes to the  $C_{60}$  rotational state populations. Unfortunately, during these experiments we were unable to complete a second temperature cycle to isolate the reversible temperature dependences completely.

Nonetheless, the qualitative resemblance between the simulated spectra and difference trace in Figure 4, vs. the experimental data for the  $F_{1u}(2)$  and  $F_{1u}(3)$  modes in Figures 6 and 7, supports the notion that some fraction of the  $C_{60}$  molecules may exist as slightly hindered rotors.

However, the relatively small magnitudes of the thermally induced changes in the experimental spectra, as compared to the large effects predicted by the simulations, implies that at most only a small fraction of the C<sub>60</sub> molecules can rotate. Further constraining this interpretation is the narrow (0.2 cm<sup>-1</sup> FWHM) linewidth and apparent temperature independence of the  $F_{lu}(1)$  mode shown in Figure 5, for which the expected P and R-branches are not apparent. This spectrum implies that none of the C<sub>60</sub> molecules are capable of rotating.

Clearly, thermally induced rotational population changes, and the slightly hindered rotor C<sub>60</sub> molecules they imply, cannot be completely ruled out given the present data. A final determination of the influences of <sup>13</sup>C isotopic substitution, pH<sub>2</sub> matrix effects, and the C<sub>60</sub> rotational state distribution on the observed C<sub>60</sub>/pH<sub>2</sub> bandshapes awaits further experimentation and analysis. We are preparing to conduct a new study involving the deposition of <sup>13</sup>C depleted and enriched C<sub>60</sub> into various cryogenic matrix hosts using a range of different deposition conditions. Any informative results will be published at a later time.

In addition to the direct dopant IR absorptions, dopant-induced IR features are observed in our C<sub>60</sub>/pH<sub>2</sub> samples, as shown in Figure 9. The best known example of this phenomenon is the Q<sub>1</sub>(0) line at 4153 cm<sup>-1</sup> induced by oH<sub>2</sub> impurities.<sup>75,76,95-97</sup> We have observed similar dopant induced IR activity for a number of atomic and molecular dopant species.<sup>75,98</sup> A general model for assigning these spectra is still being developed. However the complexity of the induced IR spectra appears to increase in the dopant sequence: atomic, diatomic, polyatomic; perhaps reflecting the increasing number of dissimilar environments, and hence Stark shifts, experienced by the participating pH<sub>2</sub> molecules. If so, then the complexity of the C<sub>60</sub>-induced spectrum implies a large number of dissimilar environments for the surrounding pH<sub>2</sub> molecules. Any "complete" model of C<sub>60</sub>/pH<sub>2</sub> trapping site structure(s) would have to explain these data as well as the direct IR absorption lineshapes.

We note that the total integrated intensity of the induced IR spectrum is comparable in magnitude to that of the direct C<sub>60</sub> absorptions; we estimate  $\int \alpha_{ind}(\bar{\nu}) d\bar{\nu} \approx 7 \text{ km/mol}$ , where the corresponding concentration is that of the C<sub>60</sub> dopant.<sup>94</sup> Thus, we propose this induced IR phenomenon as a diagnostic for probing the chemical environments of pH<sub>2</sub> molecules adsorbed by carbon nanotubes at cryogenic temperatures. If experimental conditions can be arranged to observe the nanotube IR absorptions, then we predict that the nanotube-induced IR activity in the

adsorbed  $\text{pH}_2$  molecules should also be measurable. This technique has recently been applied to characterize the electric fields experienced by  $\text{H}_2$  molecules adsorbed in zeolites.<sup>99</sup>

Figure 10 shows a portion of the visible absorption spectrum of the as-deposited  $\text{C}_{60}/\text{pH}_2$  sample depicted in Figures 6-8. The spectral features are similar to, but somewhat broader than, those observed in previous molecular beam,<sup>28</sup> helium droplet,<sup>29</sup> and Ne matrix studies.<sup>33,34</sup> The observed spectral linewidths do not appear to be limited by the  $\approx 0.8 \text{ nm}$  ( $\approx 20 \text{ cm}^{-1}$ ) experimental resolution. The sharp peaks observed in this spectrum further support our assignment of the spectra presented in this section to isolated  $\text{C}_{60}$  molecules.

## B. $\text{C}_{60}$ Clusters

Solid  $\text{pH}_2$  samples produced by the enclosed cell condensation method have a predominantly hcp microscopic structure.<sup>67,73</sup> Consequently, inhomogeneities in dopant molecule environments should be reduced in cell condensed doped  $\text{pH}_2$  samples, an important advantage over rapid vapor deposited samples which are mixed fcc and hcp. For example, the linewidths of the  $\nu_4$   $\text{CH}_4$  absorptions in cell condensed  $\text{CH}_4/\text{pH}_2$  samples are measurably smaller than in annealed rapid vapor deposited samples.<sup>77</sup> Unfortunately, the same elevated sample preparation temperature which leads to formation of the thermodynamically stable pure hcp phase, also results in greatly increased clustering of the dopant molecules.

Figure 11 shows an IR absorption spectrum of laser vaporized  $\text{C}_{60}$  trapped in solid  $\text{pH}_2$  grown in an enclosed cell. The peaks at  $1184.3$  and  $1431.8 \text{ cm}^{-1}$  are identified as the  $F_{1u}(3)$  and  $F_{1u}(4)$  IR active fundamentals of  $\text{C}_{60}$ , respectively. The strong peak at  $1167.1 \text{ cm}^{-1}$ , and the broad band ranging from  $1200$  to  $1500 \text{ cm}^{-1}$ , are due to the  $\text{U}_0(0)$  transition of solid  $\text{pH}_2$  and its phonon sideband, respectively.<sup>100</sup> The sharp peak at  $1308 \text{ cm}^{-1}$  corresponds to the  $\nu_4$  mode of  $\text{CH}_4$ . Not shown is a sharp peak at  $2034.4 \text{ cm}^{-1}$  which is due to the  $\nu_3$  mode<sup>69</sup> of  $\text{C}_3$ . These smaller carbon-containing species are formed by photofragmentation of the  $\text{C}_{60}$  by the ablation laser, and, in the case of  $\text{CH}_4$ , by subsequent reactions with the  $\text{pH}_2$  host. The sharp spikes in the  $1380$  to  $1500 \text{ cm}^{-1}$  region are due to inexact cancellation of absorptions by water vapor in the laboratory air.

Figure 12 shows the absorption lineshapes of the  $F_{1u}(3)$  and  $F_{1u}(4)$  modes in greater detail. The dotted traces are recorded at a higher resolution of  $0.01 \text{ cm}^{-1}$ , while the solid traces are taken at a resolution of  $0.25 \text{ cm}^{-1}$ . The spectrum of the  $F_{1u}(3)$  mode consists of two components: one



peaking at  $1184.3\text{ cm}^{-1}$ , and a shoulder at  $1183.2\text{ cm}^{-1}$ . The spectrum of  $F_{1u}(4)$  is more difficult to deconvolve into multiple components, but shows signs of a long red-degraded tail. Both spectra appear to be broadened versions of the  $C_{60}$  monomer  $F_{1u}(3)$  and  $F_{1u}(4)$  mode spectra presented above in Figures 7 and 8. The additional line broadening is probably due to a higher extent of clustering of the  $C_{60}$  molecules in the enclosed cell grown sample.

The spectral peak positions and linewidths observed for both the rapid vapor deposited, and enclosed cell grown  $C_{60}/pH_2$  samples, are collected in Table I, along with other values gleaned from the literature. The two sets of  $C_{60}/pH_2$  data agree well with each other, and for the most part with the peak positions reported for a  $C_{60}/Ar$  sample<sup>41</sup> at  $T = 10\text{ K}$  (except for the  $F_{1u}(2)$  mode which shows a discrepancy of about  $1.0\text{ cm}^{-1}$ ). However, the  $C_{60}/pH_2$  peak positions and qualitative lineshapes do not agree well with the solid  $C_{60}$  data, even for solid  $C_{60}$  temperatures below the orientational glass transition temperature<sup>51</sup> of  $\approx 90\text{ K}$ . Specifically: the position of the  $F_{1u}(3)$  mode peak, and the number of peaks observed for the  $F_{1u}(4)$  mode, are different for enclosed cell grown  $C_{60}/pH_2$  solids and low temperature  $C_{60}$  films. These results show that the  $(C_{60})_n$  clusters in the  $C_{60}/pH_2$  sample are too small to exhibit "bulk" solid  $C_{60}$  vibrational behavior.

Figure 13 shows a UV/visible absorption spectrum of the enclosed cell grown  $C_{60}/pH_2$  sample. The spectrum is dominated by three bands peaking at 211, 257, and 334 nm, followed by a broad hump ranging in the 380 to 500 nm region. A relatively narrow absorption feature at 405 nm is superimposed on this broad hump (see the inset in Figure 13). A tailing absorption starting near 500 nm spans up to 700 nm. (Note that the absorption intensities below  $\approx 250\text{ nm}$  should not be compared quantitatively with other regions because of significant wavelength dependent light scattering by the matrix.)

The main bands at 211, 257, and 334 nm in Figure 13 are identified as dipole allowed electronic transitions of  $C_{60}$ ; similar bands have been reported for both  $C_{60}$  in solution<sup>35,36</sup> and for thin films<sup>6</sup> of solid  $C_{60}$ . Isolated  $C_{60}$  also exhibits two sharp peaks at around 405 nm separated by  $\approx 4\text{ nm}$ , as has been observed for isolated  $C_{60}$  in the gas phase,<sup>28</sup> in solution,<sup>36</sup> and in cold matrices.<sup>28,36</sup> However, the absorption at 405 nm in Figure 13 has only one peak with a much broader linewidth than expected for isolated  $C_{60}$ . Moreover, the broad hump in the 380 to 500 nm region is a characteristic feature of  $C_{60}$  thin films<sup>6</sup> but not of  $C_{60}$  in solution.<sup>35,36</sup> Therefore, the observation of the hump in Figure 13 indicates that the  $C_{60}$  molecules in the enclosed cell

grown sample are not completely isolated. Finally, the structureless tailing absorption in the 500 to 700 nm region seen in Figure 13 is not compatible with the structure-rich spectra observed for isolated  $C_{60}$  at low temperatures,<sup>28,29,34</sup> as typified by the  $C_{60}/pH_2$  spectrum in figure 10.

Both the IR and UV/visible observations indicate that  $C_{60}$  molecules are not well isolated in the enclosed cell grown  $C_{60}/pH_2$  sample. However, the spectroscopy does not match that expected for cryogenic bulk  $C_{60}$ , either. A natural interpretation is that the laser ablation process produces  $(C_{60})_n$  clusters that are trapped intact in the matrix. Cluster beams of  $(C_{60})_n$  are reported by mass spectroscopy of laser vaporized thin films of  $C_{60}$  in a supersonic helium-gas expansion source.<sup>101</sup> Even under vacuum, laser ablation of  $C_{60}$  results in coalescence of the molecules to give higher mass peaks of  $(C_{60})_n$ .<sup>102,103</sup>

Thus, it appears that in this instance the spectral broadening due to  $C_{60}$  cluster formation overwhelms the inherent advantage of pure hcp solid  $pH_2$  structure formation, resulting in broader observed lines for enclosed cell grown samples than for rapid vapor deposited samples.

## VI. SUMMARY AND FUTURE DIRECTIONS

We have performed theoretical simulations of rotationally resolved rovibrational spectra of isolated  $C_{60}$  molecules at liquid helium temperatures, including the effects of boson-exchange symmetry restrictions on the rotational levels of the icosahedral  $^{12}C_{60}$  molecule. The simulations predict a characteristic "null gap" and unequal rotational line spacings for low- $J$  values as a consequence of the symmetry forbidden missing rotational levels.

We have successfully isolated  $C_{60}$  molecules in cryogenic  $pH_2$  solids using the rapid vapor deposition sample preparation method. High resolution IR absorption spectra of these samples fail to show rotationally resolved features, and suggest that the majority of the  $C_{60}$  molecules cannot rotate. However, spectra of the  $F_{1u}(\bar{1})$  vibrational mode show peaks with linewidths of  $\approx 0.2 \text{ cm}^{-1}$  FWHM, the sharpest IR absorption bands for  $C_{60}$  reported to date. Visible absorption spectra show sharp features in the  $\approx 600 \text{ nm}$  region, supporting our contention that the  $C_{60}$  molecules are well isolated.

The presence of the  $C_{60}$  molecules in the  $pH_2$  solid appears to inhibit the fcc to hcp conversion typically observed upon annealing to  $T \approx 5 \text{ K}$ . We propose that this is due to the multi-substitutional nature of the  $C_{60}$  trapping site; the large guest molecule protrudes into adjacent close packed planes and precludes their relative slipping motion. Efforts to generate

sharper  $C_{60}/pH_2$  IR absorptions should thus focus on the initial sample preparation phase, rather than on post-deposition processing.

We have observed IR absorptions of the  $pH_2$  molecules induced by the presence of the  $C_{60}$  molecules. We are thus encouraged to continue our efforts to better understand  $C_{60}/pH_2$  and more general fullerene- $H_2$  interactions. The integrated absorption strength of the induced feature is comparable to those of the direct  $C_{60}$  IR absorptions. We propose that this phenomenon can be used as a diagnostic of the chemical environments experienced by hydrogen molecules adsorbed by carbon nanotubes at cryogenic temperatures.

$C_{60}/pH_2$  samples grown in an enclosed cell by laser ablation of solid  $C_{60}$  appear to contain predominantly  $(C_{60})_n$  clusters, as determined by IR and UV/visible absorption spectroscopies. These clusters are of insufficient size to exhibit true "bulk" vibrational and electronic spectra, yet still large enough to result in considerable line broadening as observed for the  $F_{1u}(3)$  and  $F_{1u}(4)$  modes. Our previous experience with  $(CH_4)_n$  clusters in  $pH_2$  suggests that high resolution laser spectroscopic techniques may be capable of resolving sharp spectral features overlaying the broad IR absorption peaks.<sup>72</sup> Spectra of  $(C_{60})_n$  clusters in solid  $pH_2$  should ultimately yield important information about the  $C_{60}$ - $C_{60}$  interactions.

We have not disentangled the contributions of  $^{13}C$  isotopic substitution,  $pH_2$  matrix effects, and the putative hindered rotation of  $C_{60}$  molecules to the observed  $C_{60}/pH_2$  IR lineshapes. We are preparing for matrix isolation experiments on  $^{13}C$  depleted and enriched  $C_{60}$  samples in a variety of matrix hosts. We hope that ultimately these efforts will illuminate the structure and vibrational dynamics of the  $C_{60}$  molecule via the observation of a rotationally resolved rovibrational spectrum.

## ACKNOWLEDGEMENTS

The study in Kyoto was partially supported by Grant-in-Aid for Scientific Research of the Ministry of Education, Science, Culture and Sports of Japan. The authors thank Dr. J.A. Sheehy for a critical reading of the manuscript.

## REFERENCES

- (1) Chemical Abstracts Service, American Chemical Society.
- (2) Jones, D.E.H. (Daedalus) New Scientist **1966**, 32, 245; see also discussion in:  
Kroto, H. Science **1988**, 242, 1139.
- (3) Osawa, E. Kagaku (Kyoto) **1970**, 25, 854; in Japanese.
- (4) Rohlffing, E.A.; Cox, D.M.; Kaldor, A. J. Chem. Phys. **1984**, 81, 3322.
- (5) Kroto, H.W.; Heath, J.R.; O'Brien, S.C.; Curl, R.F.; Smalley, R.E.  
Nature **1985**, 318, 162.
- (6) Kratschmer, W.; Lamb, L. D.; Fostiropoulos, K.; Huffman, D. R.  
Nature **1990**, 347, 354.
- (7) Iijima, S. Nature **1991**, 354, 56.
- (8) Iijima, S.; Ichihashi, T. Nature **1993**, 363, 603.
- (9) McLafferty, F.W., Ed.; Acc. Chem. Res. **1992**, 25, 97;  
"Special Issue on Buckminsterfullerenes."
- (10) Dresselhaus, M. S.; Dresselhaus, G.; and Eklund, P. C.  
Science of Fullerenes and Nanotubes; Academic Press: New York, 1996; ISBN 0-12-221820-5.
- (11) Leach, S., Ed.; J. Phys. B **1996**, 29, 4855;  
"Special Issue on Fullerenes: Atomic, Molecular and Optical Physics."
- (12) Ebbesen, T.W. Carbon Nanotubes: Preparation and Properties;  
CRC Press: Boca Raton, 1997.
- (13) Weeks, D.E.; Harter, W.G. Chem. Phys. Lett. **1991**, 176, 209.
- (14) Weeks, D.E. J. Chem. Phys. **1992**, 96, 7380.
- (15) Dixon, D.A.; Chase, B.E.; Fitzgerald, G.; Matsuzawa, N.  
J. Phys. Chem. **1995**, 99, 4486.
- (16) Varga, F.; Nemes, L.; Watson, J.K.G. J. Phys. B **1996**, 29, 5043.
- (17) Negri, F.; Orlandi, G. J. Phys. B **1996**, 29, 5049.
- (18) Heid, R.; Pintschovius, L.; Godard, J.M. Phys. Rev. B **1997**, 56, 5925.
- (19) Dillon, A.C.; Jones, K.M.; Bekkedahl, T.A.; Kiang, C.H.; Bethune, D.S.;  
Heben, M.J. Nature **1997**, 386, 377.
- (20) Vidales, A.M.; Crespi, V.H.; Cole, M.W. Phys. Rev. B. **1998**, 58, R13426.
- (21) Wang, Q.; Johnson, J.K. J. Chem. Phys. **1999**, 110, 577.

- (22) Harter, W.G.; Reimer, T.C. Chem. Phys. Lett. **1992**, 194, 230.
- (23) Saito, R.; Dresselhaus, G.; Dresselhaus, M.S. Phys. Rev. B **1994**, 50, 5680.
- (24) Reimer, T.C.; Harter, W.G. J. Chem. Phys. **1997**, 106, 1326.
- (25) Edwards, S.A.; Leach, S. Astron. Astrophys. **1993**, 272, 533.
- (26) Nemes, L. J. Mol. Struct. **1997**, 436, 25.
- (27) Frum, C.I.; Engleman, R., Jr.; Hedderich, H.G.; Bernath, P.F.; Lamb, L.D.; Huffman, D.R. Chem. Phys. Lett. **1991**, 176, 504.
- (28) Haufler, R.E.; Chai, Y.; Chibante, L.P.F.; Fraelich, M.R.; Weisman, R.B.; Curl, R.F.; Smalley, R.E. J. Chem. Phys. **1991**, 95, 2197.
- (29) Close, J.D.; Federmann, F.; Hoffmann, K.; Quaas, N. Chem. Phys. Lett. **1997**, 276, 393.
- (30) Gasyna, Z.; Schatz, P.N.; Hare, J.P.; Dennis, T.J.; Kroto, H.W.; Taylor, R.; Walton, D.R.M. Chem. Phys. Lett. **1991**, 183, 283.
- (31) Sassara, A.; Zerza, G.; Chergui, M. Chem. Phys. Lett. **1996**, 261, 213.
- (32) Hung, W.C.; Ho, C.D.; Liu, C.P.; Lee, Y.P. J. Phys. Chem. **1996**, 100, 3927.
- (33) Sassara, A.; Zerza, G.; Chergui, M. J. Chem. Phys. **1997**, 107, 8731.
- (34) Sassara, A.; Zerza, G.; Chergui, M.; Negri, F.; Orlandi, G. J. Chem. Phys. **1997**, 107, 8731.
- (35) Ajie, H.; Alvarez, M. M.; Anz, S. J.; Beck, R. D.; Diederich, F.; Fostiropoulos, K.; Huffman, D. R.; Kratschmer, W.; Rubin, Y.; Schriver, K. E.; Sensharma, D.; Whetten, R. L.; J. Phys. Chem. **1990**, 94, 8630.
- (36) Leach, S.; Vervloet, M.; Despres, A.; Breheret, E.; Hare, J. P.; Dennis, T. J.; Kroto, H. W.; Taylor, R.; Walton, D. R. M. Chem. Phys. **1992**, 160, 451.
- (37) Catalan, J. Chem. Phys. Lett. **1994**, 223, 159.
- (38) Smith, A.L. J. Phys. B **1996**, 29, 4975.
- (39) Coheur, P.F.; Carleer, M.; Colin, R. J. Phys. B **1996**, 29, 4987.
- (40) van den Heuvel, D.J.; van den Berg, G.J.B.; Groenen, E.J.J.; Schmidt, J.; Holleman, I.; Meijer, G. J. Phys. Chem. **1995**, 99, 11644.
- (41) Haufler, R.E.; Conceicao, J.; Chibante, L.P.F.; Chai, Y.; Byrne, N.E.; Flanagan, S.; Haley, M.M.; O'Brien, S.C.; Pan, C.; Xiao, Z.; Billups, W.E.; Ciufolini, M.A.; Hauge, R.H.; Margrave, J.L.; Wilson, L.J.; Curl, R.F.; Smalley, R.E. J. Phys. Chem. **1990**, 94, 8634.

- (42) Bethune, D.S.; Meijer, G.; Tang, W.C.; Rosen, H.J.; Golden, W.G.; Seki, H.; Brown, C.A.; de Vries, M.S. Chem. Phys. Lett. **1991**, 179, 181.
- (43) Chase, B.; Herron, N.; Holler, E. J. Phys. Chem. **1992**, 96, 4262.
- (44) Fu, K.J.; Karney, W.L.; Chapman, O.L.; Huang, S.M.; Kaner, R.B.; Diederich, F.; Holczer, K.; Whetten, R.L. Phys. Rev. B **1992**, 46, 1937.
- (45) Huant, S.; Robert, J.B.; Chouteau, G.; Bernier, P.; Fabre, C.; Rassat, A. Phys. Rev. Lett. **1992**, 69, 2666.
- (46) Bini, R.; Procacci, P.; Salvi, P.R.; Schettino, V. J. Phys. Chem. **1993**, 97, 10580.
- (47) Horoyski, P.J.; Thewalt, M.L.W. Phys. Rev. B **1993**, 48, 11446.
- (48) Martin, M.C.; Du, X.; Kwon, J.; Mihaly, L. Phys. Rev. B **1994**, 50, 173.
- (49) Martin, M.C.; Fabian, J.; Godard, J.; Bernier, P.; Lambert, J.M.; Mihaly, L. Phys. Rev. B **1995**, 51, 2844.
- (50) Onoe, J.; Takeuchi, K. J. Phys. Chem. **1995**, 99, 16786.
- (51) Hara, T.; Onoe, J.; Takeuchi, K. J. Phys. Chem. B **1997**, 101, 9532.
- (52) Engeln, R.; von Helden, G.; van Roij, A.J.A.; Meijer, G. J. Chem. Phys. **1999**, 110, 2732.
- (53) Bethune, D.S.; Meijer, G.; Tang, W.C.; Rosen, H.J. Chem. Phys. Lett. **1990**, 174, 219.
- (54) Love, S.P.; McBranch, D.; Salkola, M.I.; Coppa, N.V.; Robinson, J.M.; Swanson, B.I.; Bishop, A.R. Chem. Phys. Lett. **1994**, 225, 170.
- (55) Horoyski, P.J.; Thewalt, M.L.W.; Anthony, T.R. Phys. Rev. Lett **1995**, 74, 194.
- (56) Akselrod, L.; Byrne, H.J.; Donovan, S.; Roth, S. Chem. Phys. **1995**, 192, 307.
- (57) Horoyski, P.J.; Thewalt, M.L.W.; Anthony, T.R. Phys. Rev. B **1995**, 52, R6951.
- (58) Horoyski, P.J.; Thewalt, M.L.W.; Anthony, T.R. Phys. Rev. B **1996**, 54, 920.
- (59) Hadjiev, V.G.; Rafailov, P.M.; Jantoljak, H.; Thomsen, C.; Kelly, M.K. Phys. Rev. B **1997**, 56, 2495.
- (60) Tam, C.N.; Wang, B.; Keiderling, T.A.; Golden, W.G. Chem. Phys. Lett. **1992**, 198, 123.
- (61) Guha, S.; Menendez, J.; Page, J.B.; Adams, G.B.; Spencer, G.S.; Lehman, J.P.; Giannozzi, P.; Baroni, S. Phys. Rev. Lett. **1994**, 72, 3359.
- (62) Guha, S.; Menendez, J.; Page, J.B.; Adams, G.B. Phys. Rev. B **1997**, 56, 15431.

- (63) Swietlik, R.; Byszewski, P.; Kowalska, E. Chem. Phys. Lett. **1996**, 254, 73.
- (64) Graja, A.; Lapinski, A.; Krol, S. J. Mol. Struct. **1997**, 404, 147.
- (65) Paci, B.; Amoretti, G.; Arduini, G.; Ruani, G.; Shinkai, S.; Suzuki, T.; Ugozzoli, F.; Caciuffo, R. Phys. Rev. B **1997**, 55, 5566.
- (66) Long, V.C.; Musfeldt, J.L.; Kamaras, K.; Schilder, A.; Schutz, W. Phys. Rev. B **1998**, 58, 14338.
- (67) Oka, T. Annu. Rev. Phys. Chem. **1993**, 44, 299.
- (68) Momose, T.; Miki, M.; Uchida, M.; Shimizu, T.; Yoshizawa, I.; Shida, T. J. Chem. Phys. **1995**, 103, 1400.
- (69) Miki, M.; Wakabayashi, T.; Momose, T.; Shida, T. J. Phys. Chem. **1996**, 100, 12135.
- (70) Momose, T. J. Chem. Phys. **1997**, 107, 7695.
- (71) Momose, T.; Miki, M.; Wakabayashi, T.; Shida, T.; Chan, M.C.; Lee, S.S.; Oka, T. J. Chem. Phys. **1997**, 107, 7707.
- (72) Momose, T.; Katsuki, H.; Hoshina, H.; Sogoshi, N.; Wakabayashi, T.; Shida, T. J. Chem. Phys. **1997**, 107, 7717.
- (73) Momose, T.; Shida, T. Bull. Chem. Soc. Jpn. **1998**, 71, 1.
- (74) Hoshina, H.; Wakabayashi, T.; Momose, T.; Shida, T. J. Chem. Phys. **1999**, 110, 5728.
- (75) Fajardo, M.E.; Tam, S. J. Chem. Phys. **1998**, 108, 4237.
- (76) Tam, S.; Fajardo, M.E. Rev. Sci. Instrum. **1999**, 70, 1926.
- (77) Tam, S.; Fajardo, M.E.; Katsuki, H.; Hoshina, H.; Wakabayashi, T.; Momose, T. J. Chem. Phys. **1999**, 111, 4191.
- (78) Herzberg, G. Molecular Spectra and Molecular Structure. Vol. II Infrared and Raman Spectra of Polyatomic Molecules; Krieger Publishing: New York, 1991.
- (79) Bunker, P. R.; Jensen, P.; Molecular Symmetry and Spectroscopy; NRC Research Press: Ottawa, 1998.
- (80) Silvera, I.F. Rev. Mod. Phys. **1980**, 52, 393.
- (81) Fajardo, M.E. J. Chem. Phys. **1993**, 98, 110.
- (82) Fajardo, M.E. J. Chem. Phys. **1993**, 98, 119.
- (83) Scharf, D.; Martyna, G.J.; Li, D.; Voth, G.A.; Klein, M.L.



J. Chem. Phys. **1993**, 99, 9013.

(84) Cheng, E.; Whaley, K.B. J. Chem. Phys. **1996**, 104, 3155.

(85) Maitland, G.C.; Rigby, M.; Smith, E.B.; Wakeham, W.A. Intermolecular Forces, Clarendon Press: Oxford, 1981.

(86) Girifalco, L.A. J. Phys. Chem. **1992**, 96, 858.

(87) Jackson, A.G. Handbook of Crystallography, Springer-Verlag: New York, 1991.

(88) Fajardo, M.E.; Carrick, P.G.; Kenney, J.W. III J. Chem. Phys. **1991**, 94, 5812.

(89) Abrefah, J.; Olander, D.R.; Balooch, M.; Siekhaus, W.J.

Appl. Phys. Lett. **1992**, 60, 1313.

(90) Baba, M.S.; Narasimhan, T.S.L.; Balasubramanian, R.; Sivaraman, N.; Mathews, C.K. J. Phys. Chem. **1994**, 98, 1333.

(91) Piacente, V.; Gigli, G.; Giustini, A.; Ferro, D. J. Phys. Chem. **1995**, 99, 14052.

(92) Berkowitz, J. J. Chem. Phys. **1999**, 111, 1446.

(93) Han, K.L.; Lu, R.C.; Lin, H.; Gallogy, E.B.; Jackson, W.M.

Chem. Phys. Lett. **1995**, 243, 29.

(94) Fajardo, M.E.; Tam, S.; unpublished data.

(95) Gush, H.P.; Hare, W.F.J.; Allin, E.J.; Welsh, H.L. Can. J. Phys. **1960**, 38, 176.

(96) Van Kranendonk, J.; Karl, G. Rev. Mod. Phys. **1968**, 40, 531.

(97) Van Kranendonk, J. Solid Hydrogen, Plenum Press: New York, 1983.

(98) Momose, T.; unpublished data.

(99) Stephanie-Victoire, F.; Cohen de Lara, E. J. Chem. Phys. **1998**, 109, 6469.

(100) Chan, M.C.; Lee, S.S.; Okumura, M.; Oka, T. J. Chem. Phys. **1991**, 95, 88.

(101) Martin, T.P.; Naher, U.; Schaber, H.; Zimmermann, U.

Phys. Rev. Lett. **1993**, 70, 3079.

(102) Yeretzian, C.; Hansen, K.; Diederich, F.; Whetten, R. L. Nature **1993**, 359, 44.

(103) Rao, A.M.; Zhou, P.; Wang, K.A.; Hager, G.T.; Holden, J. M.; Wang, Y.; Lee, W.T.; Bi, X.X.; Eklund, P.C.; Cornett, D.S.; Duncan, M.A.; Amster, I.J. Science **1993**, 259, 955.

## FIGURE CAPTIONS

Figure 1. Schematic energy levels of the upper  $F_{lu}$  and lower  $A_g$  rovibrational states of  $^{12}\text{C}_{60}$ . Due to boson-exchange symmetry restrictions many levels are missing; all allowed levels are shown up to  $J = 16$ . Only transitions that conserve the quantum number  $R$  are allowed resulting in P, Q, and R branches, which are shown by arrows.

Figure 2. Simulated gas phase IR absorption lineshape of the  $F_{lu}(3) \leftarrow A_g$  transition of  $^{12}\text{C}_{60}$  at  $T = 5.0$  K (upper panel) and  $2.5$  K (lower panel). The rotational constant is  $B = 0.0028 \text{ cm}^{-1}$  for both the upper and lower vibrational states, while the upper state Coriolis coupling constant is  $\zeta_3 = -0.319$ . The linewidth of each transition is assumed to be  $0.0033 \text{ cm}^{-1}$  ( $100 \text{ MHz}$ ) FWHM. The insets show the spectra with the intensity of the Q-branch on-scale.

Figure 3. Simulated gas phase IR absorption lineshape of the  $F_{lu}(3) \leftarrow A_g$  transition of  $^{12}\text{C}_{60}$  at  $T = 5.0$  K (upper panel) and  $2.5$  K (lower panel). The calculation differs from the one depicted in Figure 2 only in that the rotational constant of the excited  $F_{lu}$  vibrational state is assumed to be 1 % larger than in the ground state.

Figure 4. Simulated gas phase IR absorption lineshape of the  $F_{lu}(3) \leftarrow A_g$  transition of  $^{12}\text{C}_{60}$  at (a)  $T = 5.0$ , (b)  $2.5$  K, and the difference spectrum (b)-(a). The calculation is identical to the one depicted in Figure 3, except that the spectral resolution has been degraded to  $0.05 \text{ cm}^{-1}$  FWHM.

Figure 5. IR absorption spectrum (resolution =  $0.01 \text{ cm}^{-1}$ ) of  $F_{lu}(1)$  mode in rapid vapor deposited  $\text{C}_{60}/\text{pH}_2$ . Trace (a) is for the as deposited sample at  $2.4$  K, (b) warmed to  $4.8$  K, (c) recooled to  $2.4$  K, (c)-(a) effects of annealing, (c)-(b) effects of final cooldown. The sample remains at each temperature for 1 h. During the 30 minute long sample deposition the Knudsen oven temperature is  $820(\pm 10) \text{ K}$  and the  $\text{pH}_2$  inlet rate is  $25 \text{ mmol/h}$  (sample thickness growth rate  $\approx 7 \text{ }\mu\text{m/min}$ ). The final  $\text{C}_{60}$  concentration is estimated as 100 PPM, and the sample thickness as  $0.2 \text{ mm}$ .

Figure 6. IR absorption spectrum (resolution =  $0.01 \text{ cm}^{-1}$ ) of  $F_{lu}(2)$  mode in rapid vapor deposited  $\text{C}_{60}/\text{pH}_2$ . Trace (a) is for the as deposited sample at  $2.4$  K, (b) warmed to  $4.8$  K, (c)

recooled to 2.4 K, (c)-(a) effects of annealing, (c)-(b) effects of final cooldown. The sample remains at each temperature for 1 h. During the 70 minute long sample deposition the Knudsen oven temperature is  $850(\pm 10)$  K and the  $pH_2$  inlet rate is 50 mmol/h (sample thickness growth rate  $\approx 14 \mu\text{m}/\text{min}$ ). The final  $C_{60}$  concentration is estimated as 110 PPM, and the sample thickness as 1.0 mm.

Figure 7. IR absorption spectrum of  $F_{1u}(3)$  mode in rapid vapor deposited  $C_{60}/pH_2$ . Sample preparation and interrogation are described in the caption to Figure 6.

Figure 8. IR absorption spectrum of  $F_{1u}(4)$  mode in rapid vapor deposited  $C_{60}/pH_2$ . Sample preparation and interrogation are described in the caption to Figure 6.

Figure 9. IR absorption spectrum (resolution =  $0.1 \text{ cm}^{-1}$ ) of the  $pH_2$   $Q_1(0)$  dopant-induced feature in rapid vapor deposited  $C_{60}/pH_2$ . Sample preparation conditions are described in the caption to Figure 6.

Figure 10. Visible absorption spectrum (resolution =  $0.8 \text{ nm}$ ) of a  $C_{60}/pH_2$  solid. Sample preparation conditions are described in the caption to Figure 6. The peak marked "HeNe" is due to scattered HeNe laser light, and shows the instrumental resolution.

Figure 11. IR absorption spectrum (resolution =  $0.25 \text{ cm}^{-1}$ ) of a  $C_{60}/pH_2$  sample grown in an enclosed cell by laser ablation of  $C_{60}$ .

Figure 12. IR absorption spectra of the  $F_{1u}(3)$  and  $F_{1u}(4)$  modes of a  $C_{60}/pH_2$  solid grown in an enclosed cell. The dotted line shows spectra at  $0.01 \text{ cm}^{-1}$  resolution, and the solid line at  $0.25 \text{ cm}^{-1}$  resolution. Sharp spikes in the dotted spectra are due to absorptions by water in the laboratory air.

Figure 13. UV/visible absorption spectrum of a  $C_{60}/pH_2$  solid grown in an enclosed cell.

## TABLES

Table I. Absorption peaks ( $\text{cm}^{-1}$ ) and widths (FWHM) for the four IR allowed  $F_{1u}$  vibrational modes of  $\text{C}_{60}$  in: (a) annealed rapid vapor deposited  $\text{C}_{60}/\text{pH}_2$  samples, and (b) enclosed cell grown  $\text{C}_{60}/\text{pH}_2$  samples. Peak positions and widths from the literature are included for comparison (references given in square brackets).

mode	this study		literature					
	$\text{C}_{60}/\text{pH}_2$ 2.4 K (a)	$\text{C}_{60}/\text{pH}_2$ 5 K (b)	$\text{C}_{60}/\text{Ar}$ 10 K [41]	$\text{C}_{60}$ film 15 K [43]	$\text{C}_{60}$ film 80 K [50.51]	$\text{C}_{60}$ film 300 K [43]	$\text{C}_{60}$ film 300 K [50.51]	$\text{C}_{60}/\text{CS}_2$ 300 K [43]
$F_{1u}(1)$	528.37 (0.18)							
	529.77 (0.20)	n.o.	530.1 (1)	525.5 (1.6)	525.7 (2.6)	526.2 (2.7)	526.4	527.9 (2.6)
	533.6 w (0.3)							
$F_{1u}(2)$	577.6 (0.3)							
	578.05 sh							
	578.24 (0.3)	n.o.	579.3 (2)	576.5 (0.5)	576.4 (1.0)	576.1 (1.9)	575.5	577.8 (1.9)
	578.45 sh							
$F_{1u}(3)$	1182.6 w (0.5)							
	1183.45 (0.5)							
	1184.41 (0.1)	1184.3 (2.0)	1184.8 (2)	1183.7 (1.9)	1183.6 (2.0)	1183.0 (3.1)	1183.0	1182.9 (2.8)
	1184.7 (0.3)							
$F_{1u}(4)$	1427.4 w (0.2)							
	1427.9 w (0.2)							
	1428.7 (0.2)			1424.4 (1.2)	1424			
	1429.5 (0.3)			1428.4 (1.2)	1428			
	1431.9 (1.0)	1431.8 (2.5)	1431.9 (4)	1432.3 (3.1)	1432	1429.8 (4.0)	1429.5	1429.1 (3.4)
	1432.3 sh							

sh = shoulder

w = weak intensity

n.o. = not observable

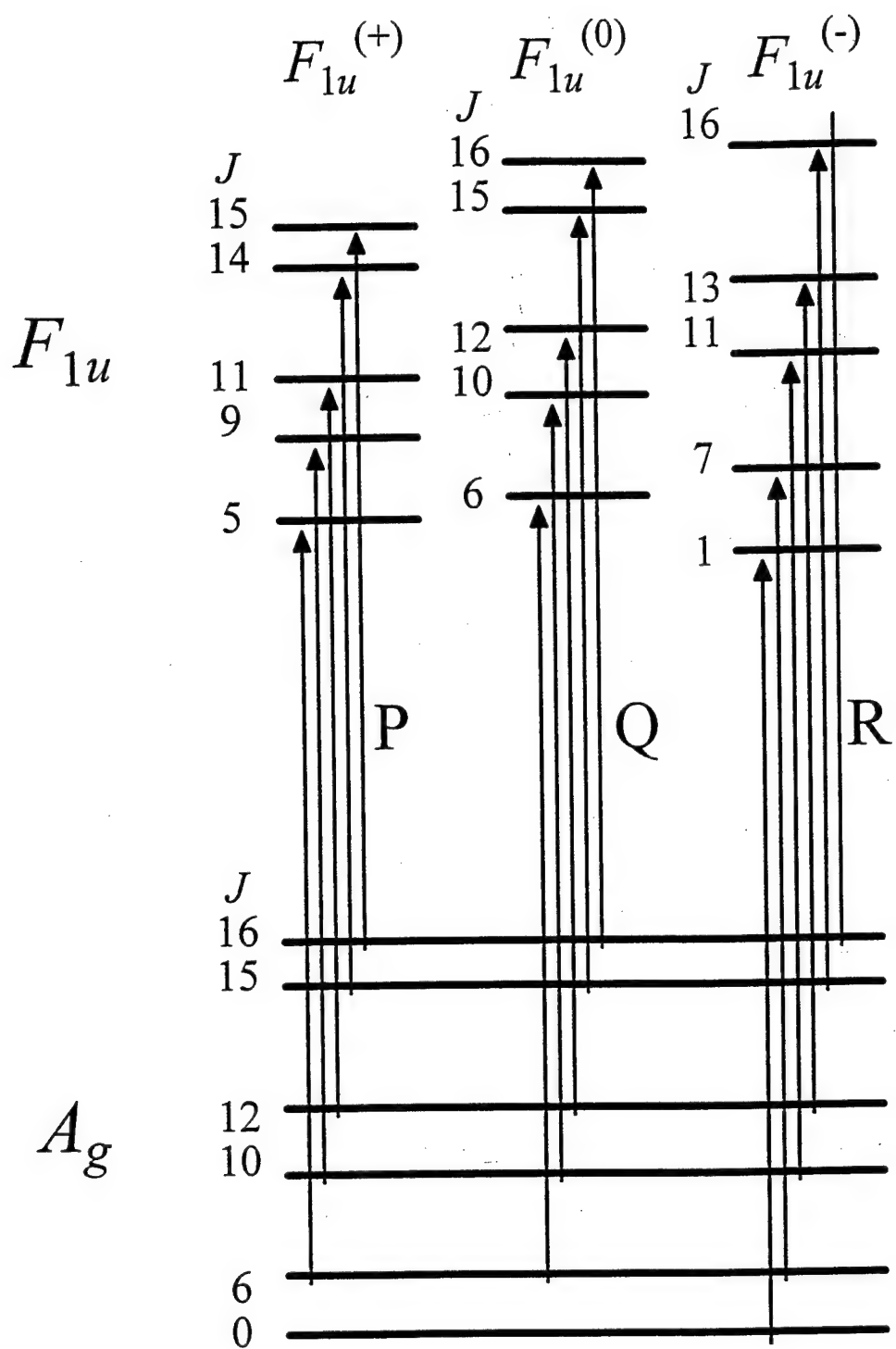


Figure 1. Sogoshi, et al.

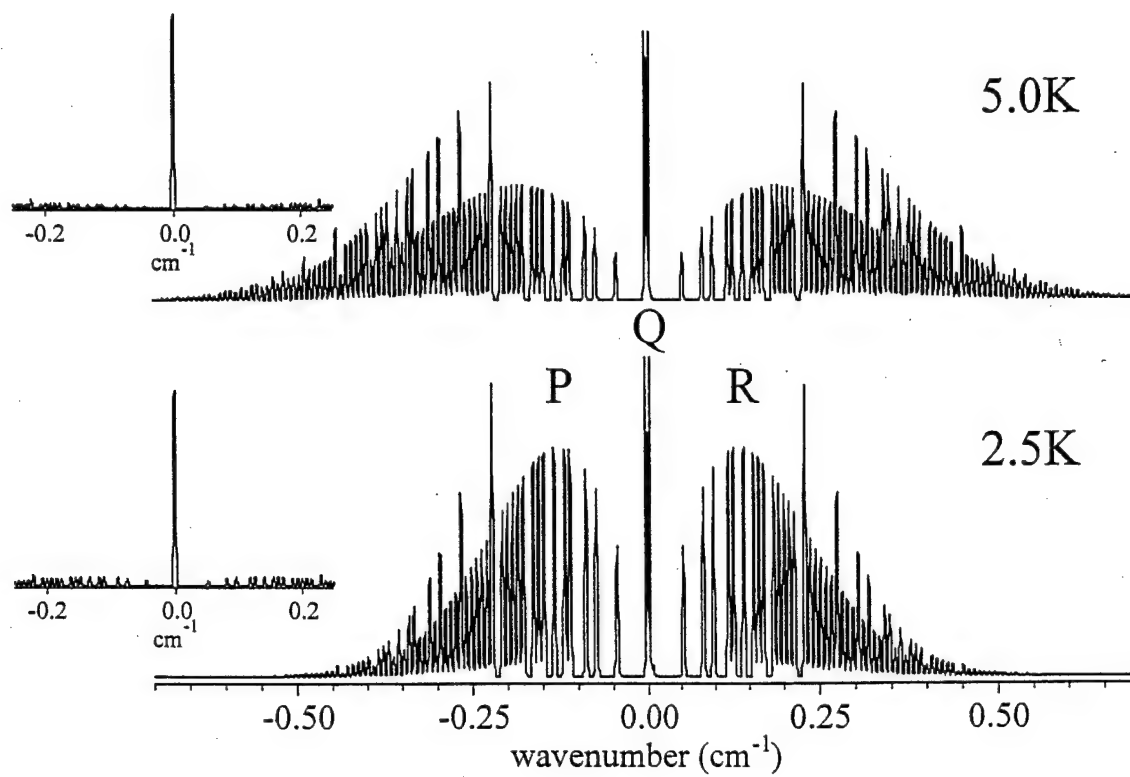


Figure 2. Sogoshi, et al.

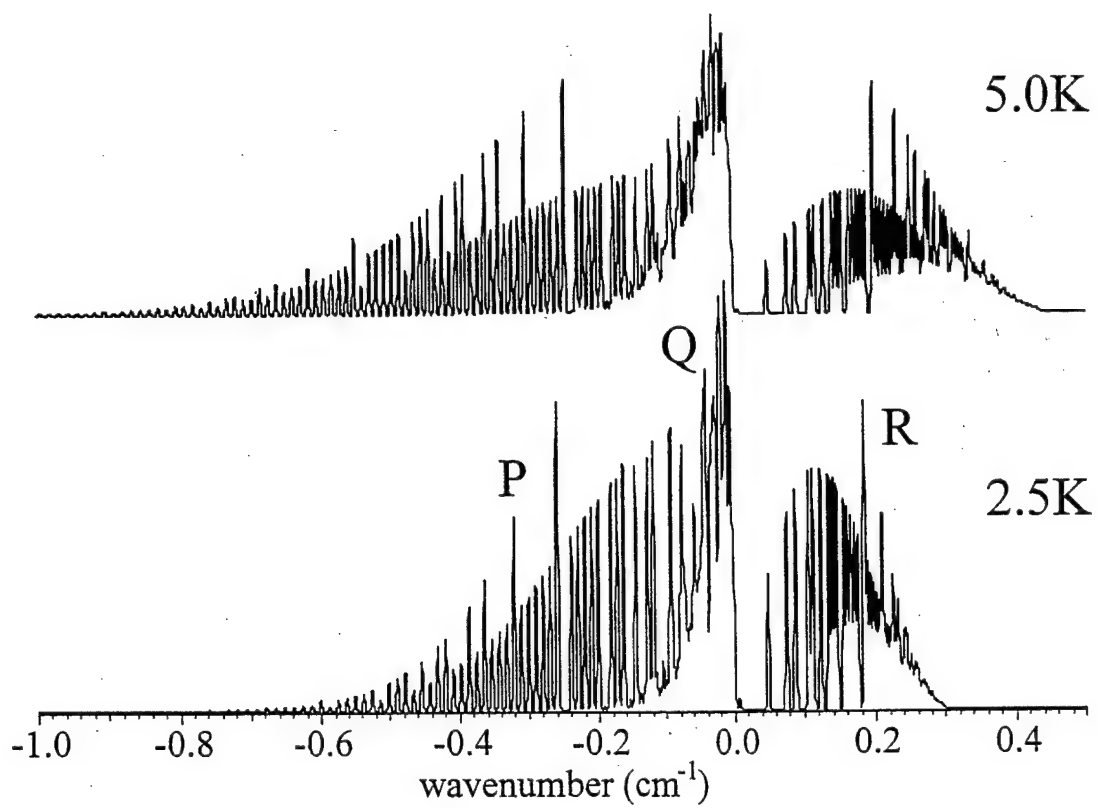


Figure 3. Sogoshi, et al.



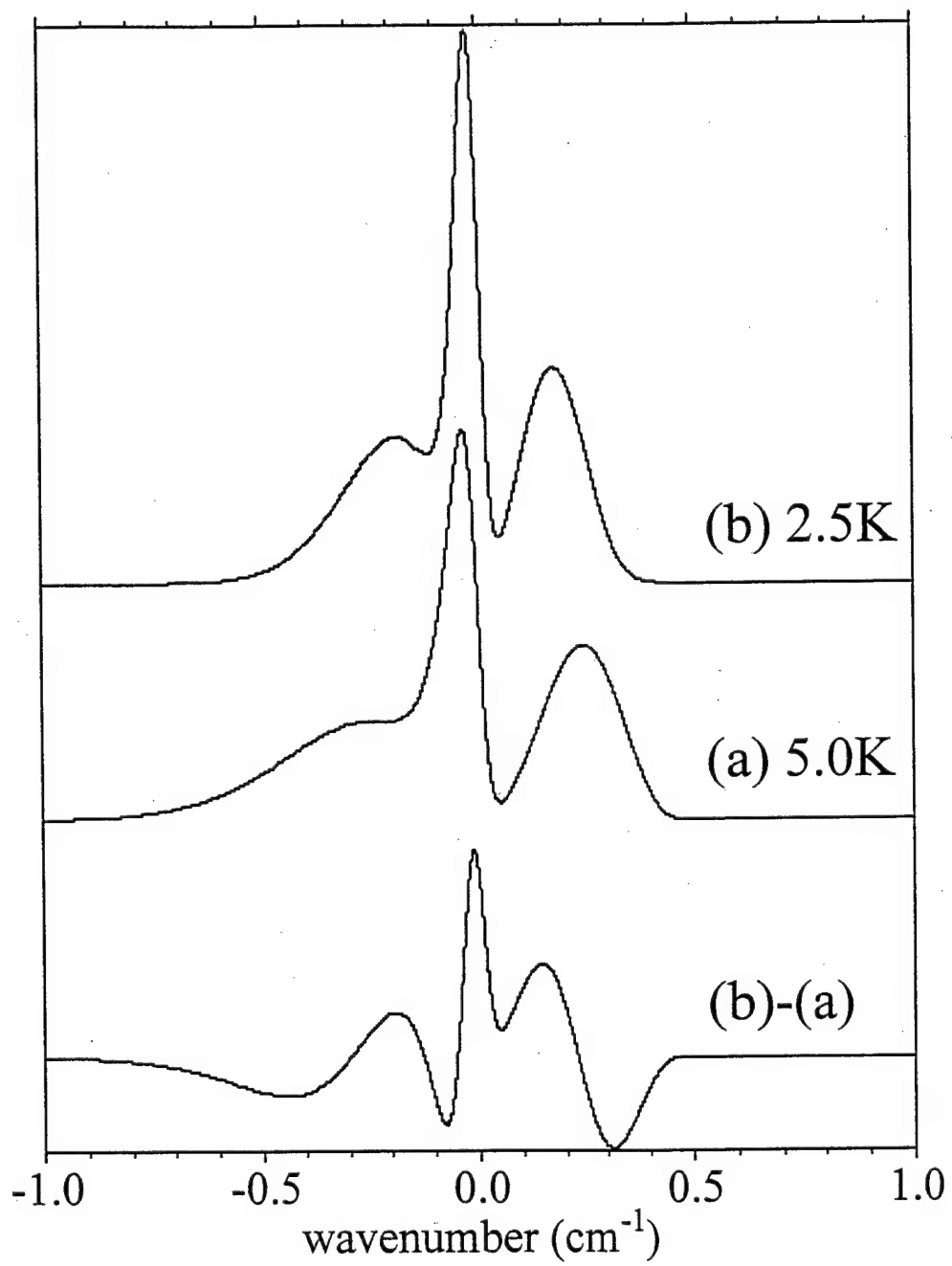


Figure 4. Sogoshi, et al.

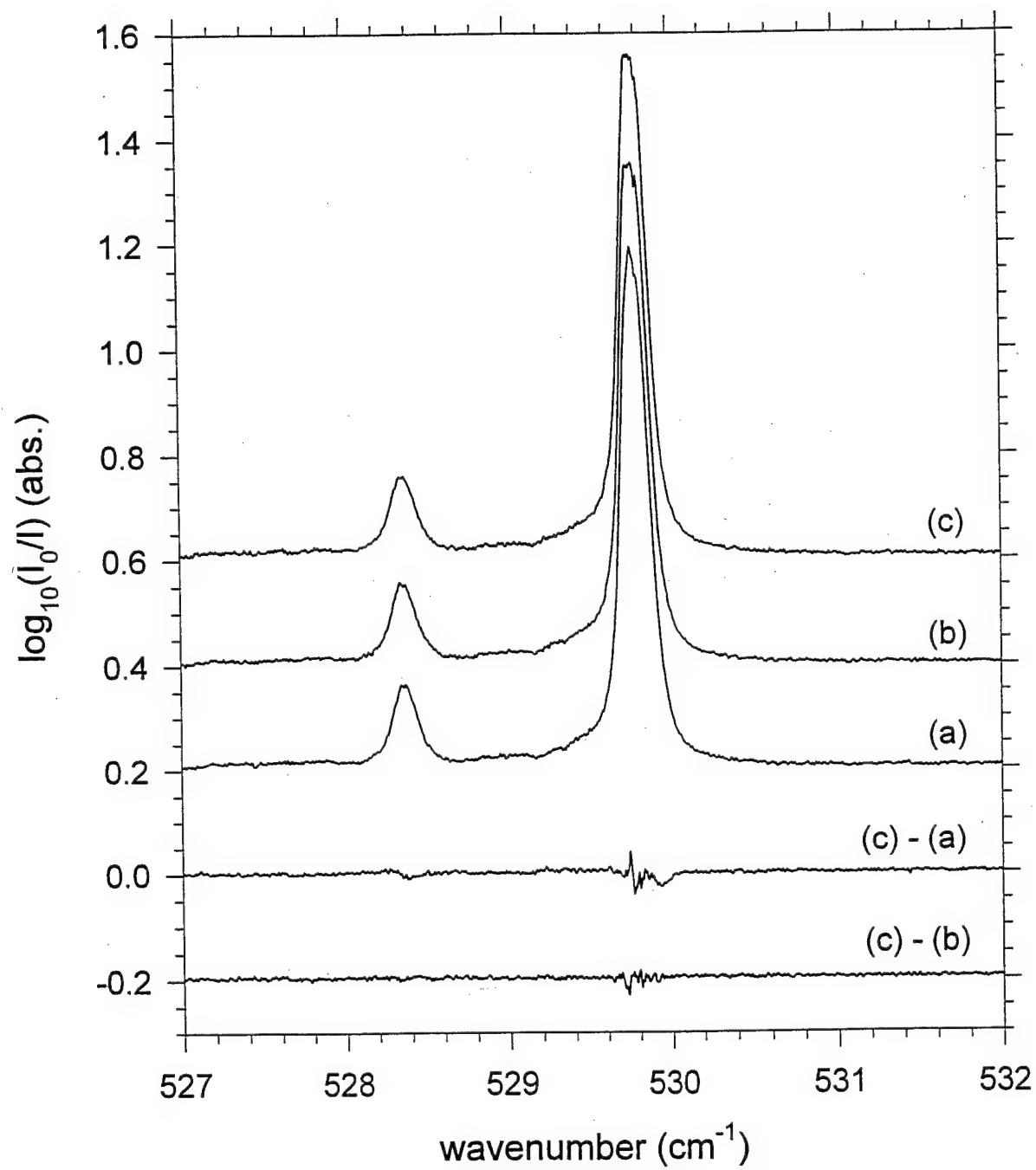


Figure 5. Sogoshi, et al.

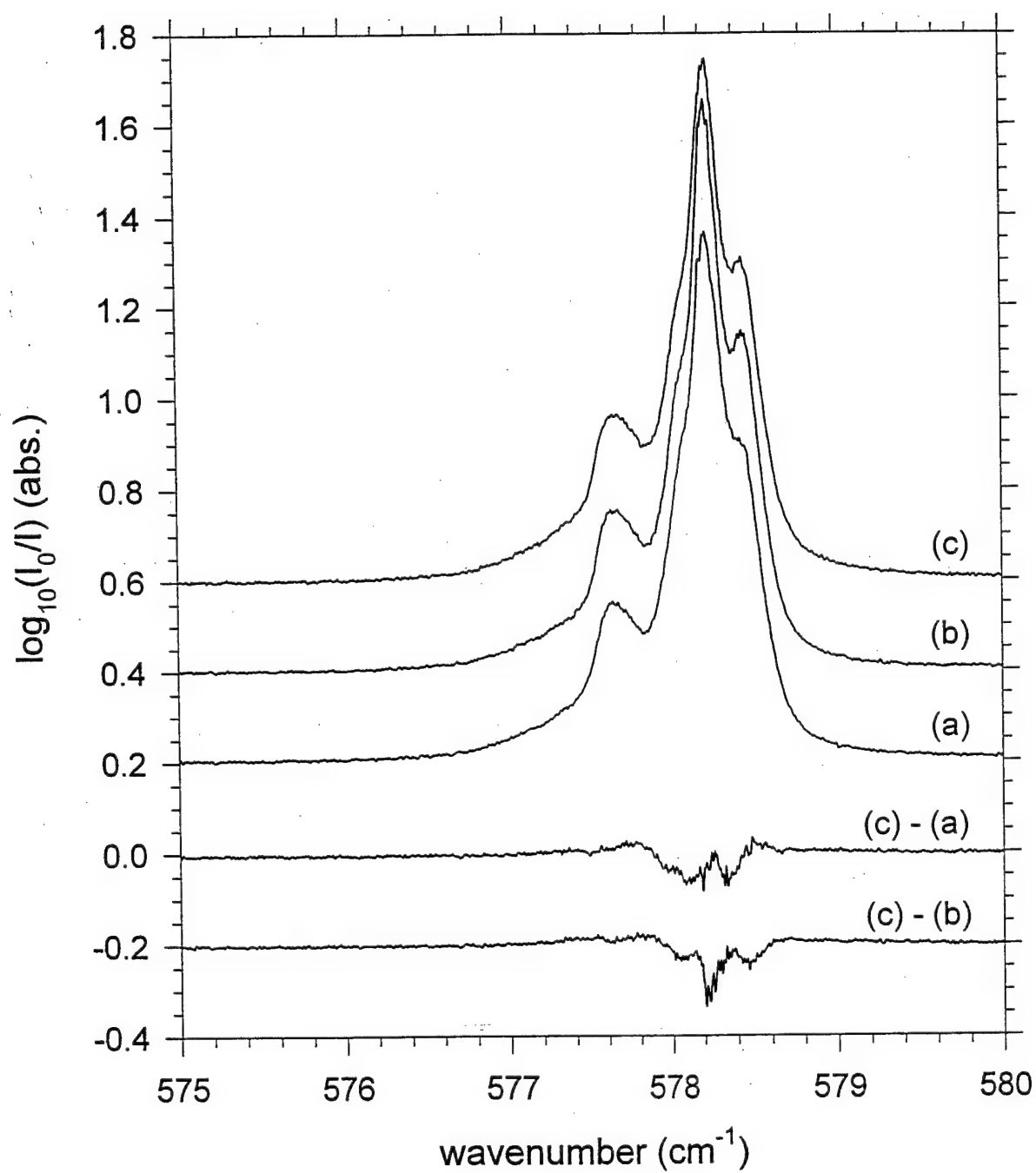


Figure 6. Sogoshi, et al.

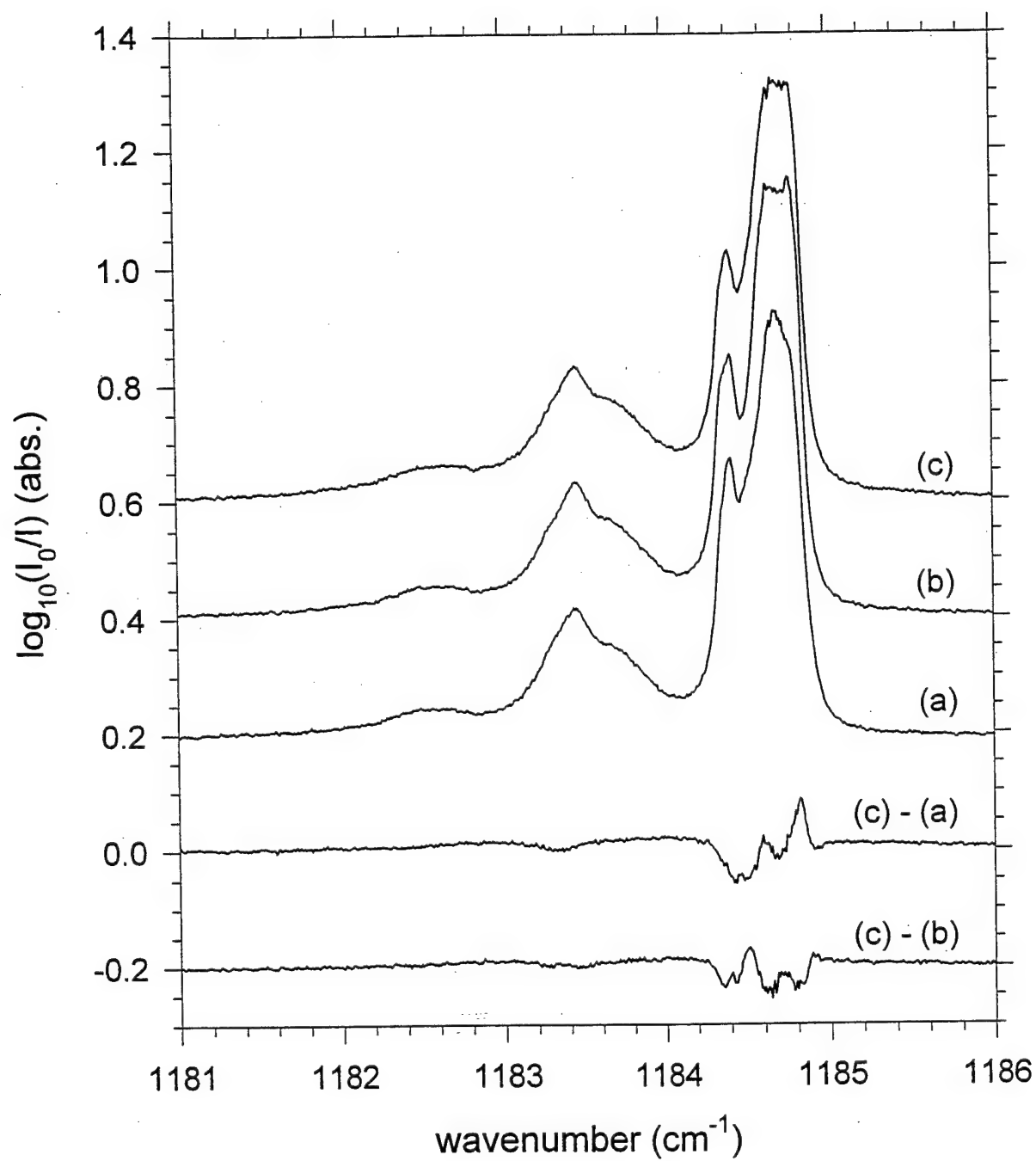


Figure 7. Sogoshi, et al.

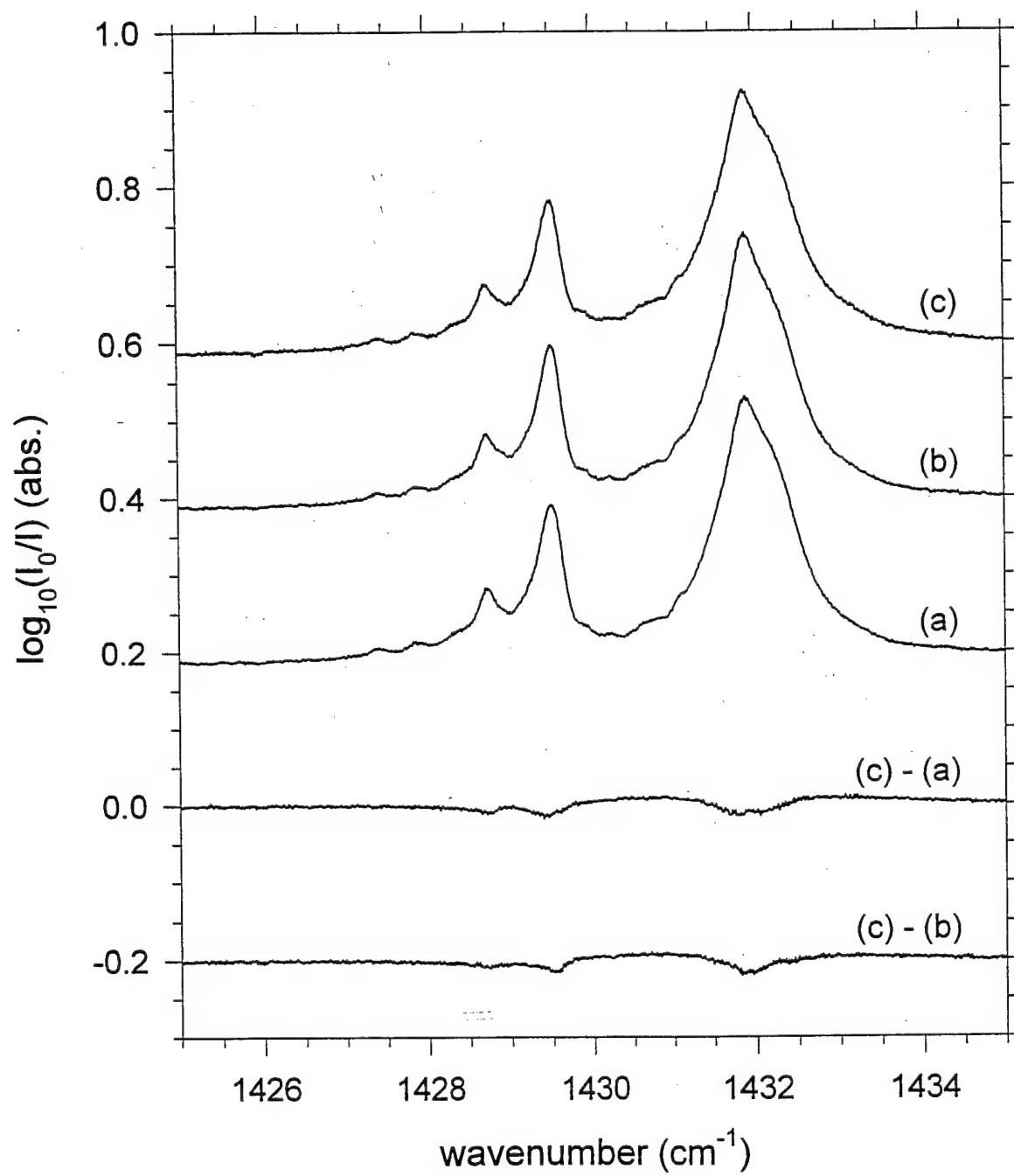


Figure 8. Sogoshi, et al.

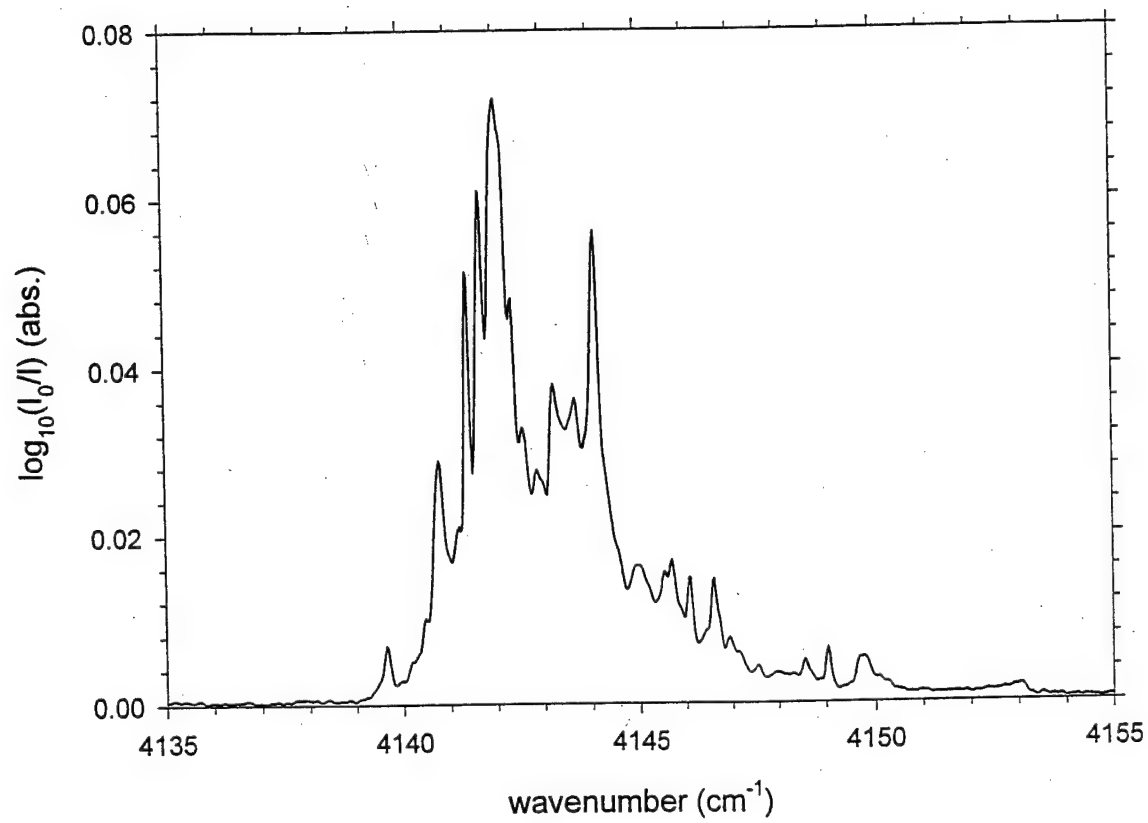


Figure 9. Sogoshi, et al.

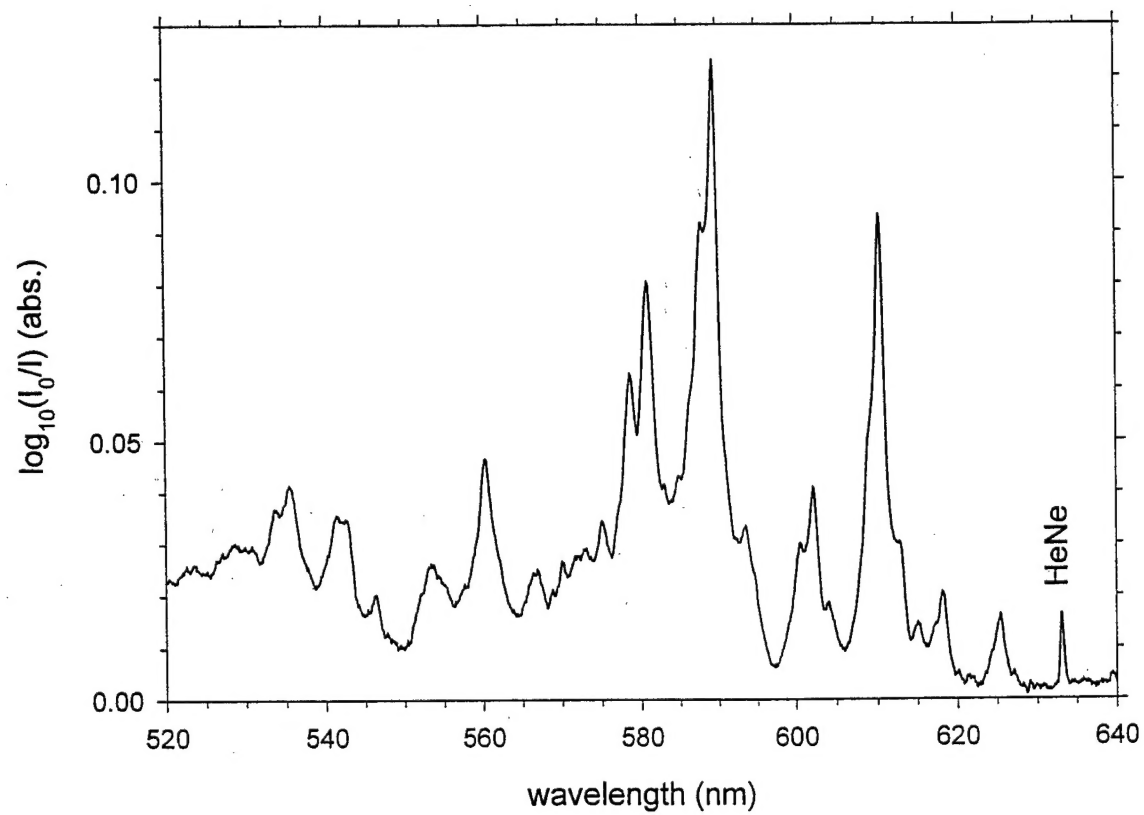


Figure 10. Sogoshi, et al.



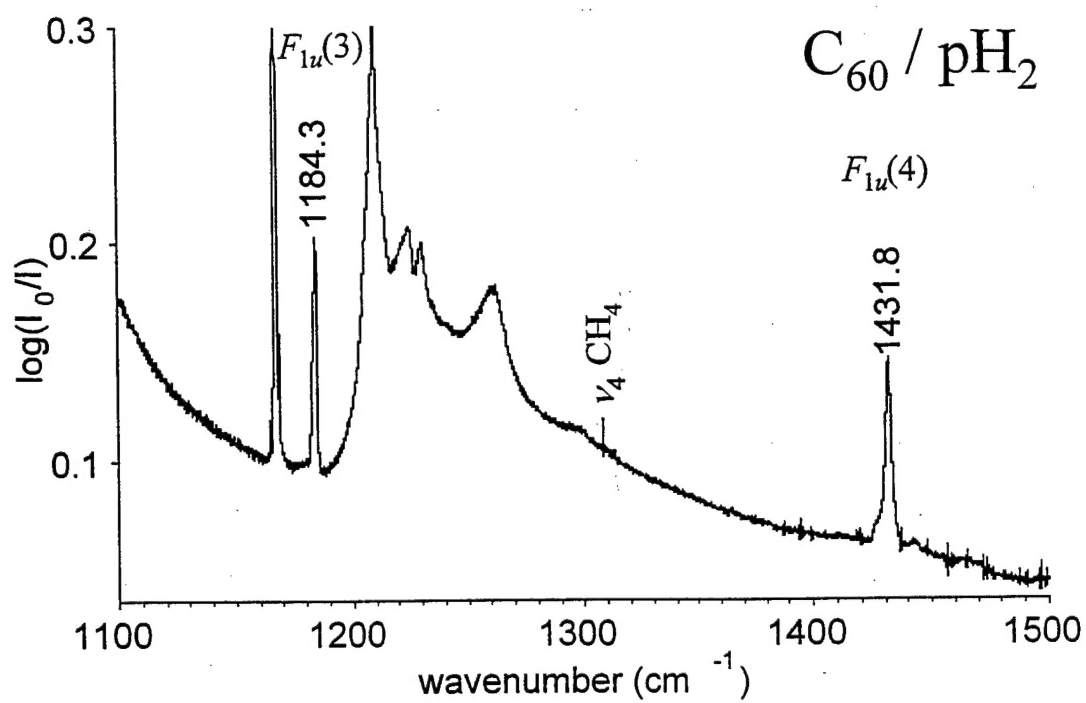


Figure 11. Sogoshi, et al.

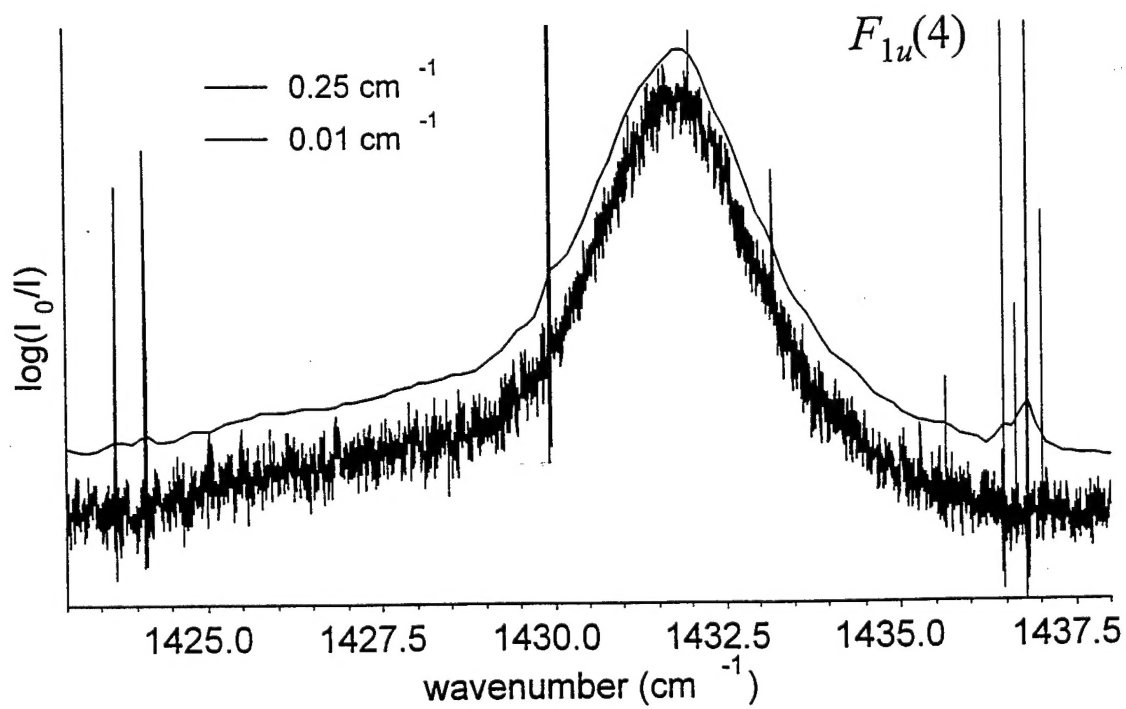
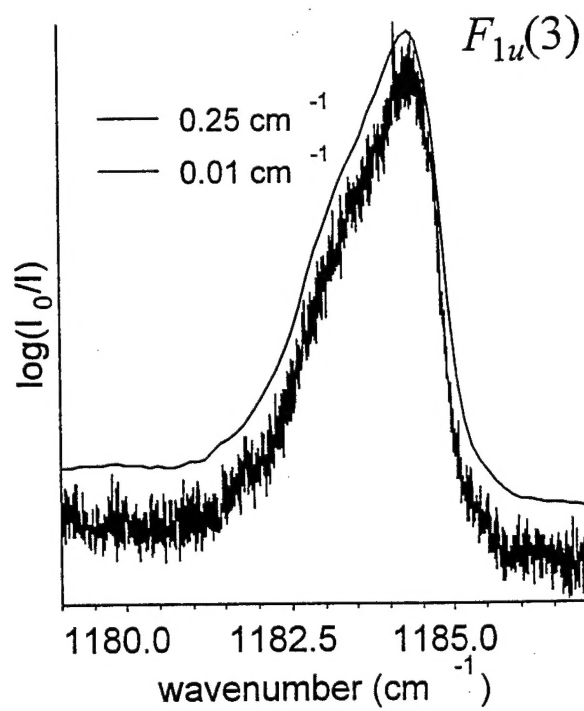


Figure 12. Sogoshi, et al.

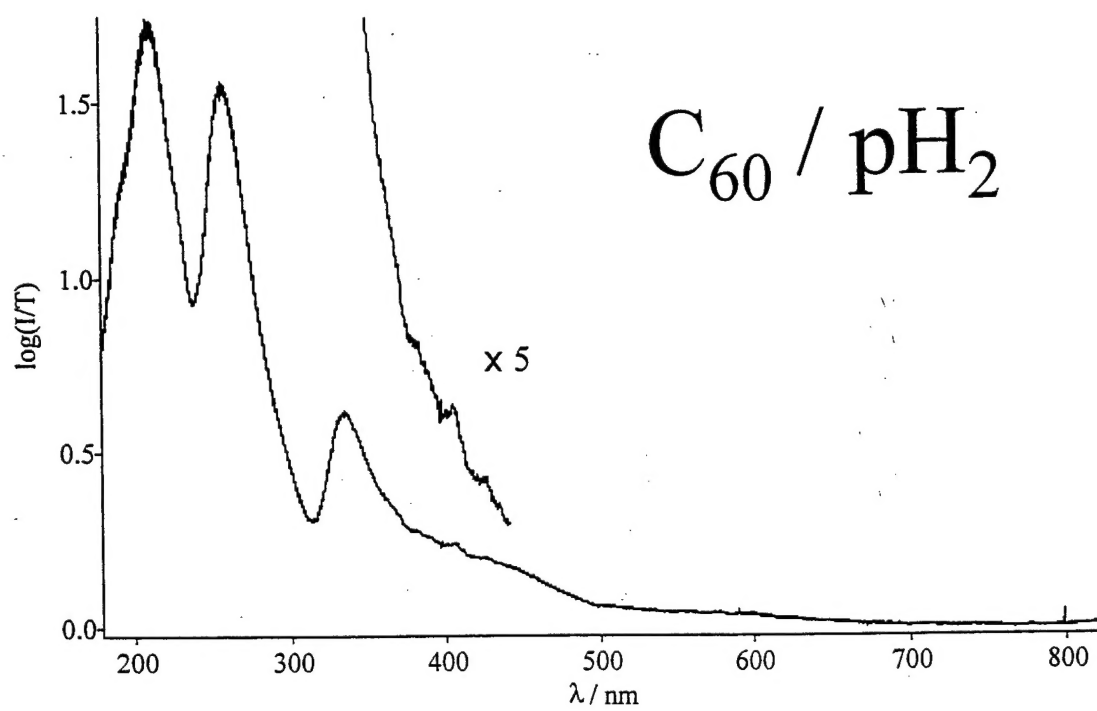


Figure 13. Sogoshi, et al.